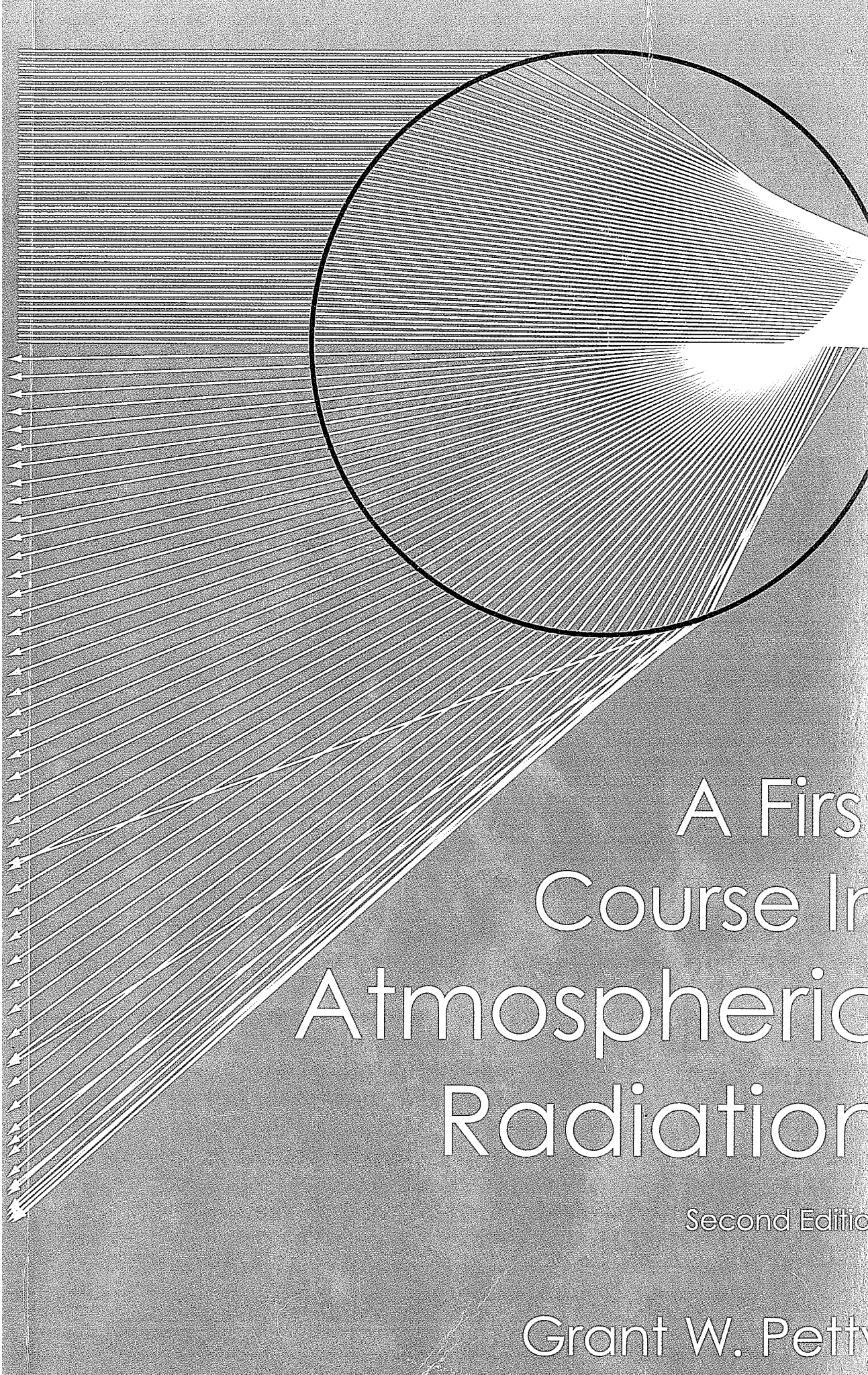

A First Course In Atmospheric Radiation

Second Edition

Grant W. Petty

CHAPTER 12

Scattering and Absorption By Particles

In the previous chapter, we introduced the mathematical framework and terminology needed to account for radiative scattering in the atmosphere. It is safe to say that whenever you find yourself struggling with a thorny problem involving radiative scattering at microwave and shorter wavelengths, some kind of *particles* are to blame, whether they be molecules or hailstones.[1]

Formally, the scattering component of the radiative transfer equation (11.9) depends on the local extinction coefficient β_e (since $d\tau = \beta_e ds$), single scatter albedo $\tilde{\omega}$ and the scattering phase function $p(\cos\Theta)$. These in turn depend both on wavelength and on the size, composition, shape and number of suspended particles, in addition to any absorption contributions by atmospheric gases. The purpose of this chapter is to examine some basic aspects of the relationship between a particle's physical and geometric properties and its absorption and scattering properties.

[1] Weak scattering can also occur at radio wavelengths due solely to turbulent fluctuations in the index of refraction of air and/or due to the presence of electrically conducting ionized gases.

Table 12.1: Examples of atmospheric particle types, with representative dimensions and number concentrations. Note that actual values can vary far more widely than indicated here.

Type	Size	Number
Gas molecule	$\sim 10^{-4}$ μm	$< 3 \times 10^{19}$ cm^{-3}
Aerosol, Aitken	< 0.1 μm	$\sim 10^{4}$ cm^{-3}
Aerosol, Large	0.1–1 μm	$\sim 10^{2}$ cm^{-3}
Aerosol, Giant	>1 μm	$\sim 10^{-1}$ cm^{-3}
Cloud droplet	5–50 μm	10^{2}–10^{3} cm^{-3}
Drizzle drop	~ 100 μm	$\sim 10^{3}$ m^{-3}
Ice crystal	10–10^{2} μm	10^{3}–10^{5} m^{-3}
Rain drop	0.1–3 mm	10–10^{3} m^{-3}
Graupel	0.1–3 mm	1–10^{2} m^{-3}
Hailstone	~ 1 cm	10^{-2}–1 m^{-3}
Insect	~ 1 cm	<1 m^{-3}
Bird	~ 10 cm	$<10^{-4}$ m^{-3}
Airplane	~ 10 m	<1 km^{-3}

12.1 Atmospheric Particles

12.1.1 Overview

The variety of particles encountered in the atmosphere is enormous. Examples include individual gas molecules, haze, smoke, dust and pollen particles, cloud droplets and ice crystals, rain drops, snowflakes, hailstones, insects, birds, and airplanes. Every one of these examples has at least some practical significance as a scatterer of EM radiation in the atmosphere.[2] Table 12.1 gives representative dimensions and number concentrations for some common atmospheric particles.

For the scattering of radiation by particles, *size matters.* The size of a particle is in fact its most important defining characteristic. In general, particles that are far smaller than the wavelength will scatter only very weakly, though they may still *absorb* radiation (e.g., the gas molecules discussed in Chapter 9). We will revisit the question of what "far smaller" means in a moment.

[2]The last three of these are significant mainly for radar.

At the other extreme, if the particle is *very large* compared to the wavelength of the radiation, then the laws of reflection, refraction, and absorption presented for homogeneous media in Chapter 4 can be used to evaluate σ_e, $\tilde{\omega}$, and $p(\Theta)$ for the particle via the approximate technique known as *ray-tracing* or *geometric optics*.[3]

Unfortunately, many particles in the atmosphere fall in between the two extremes cited above. For these particles, more complex methods are needed in order to compute their scattering and absorption properties. Such methods generally have to consider the effects of diffraction, constructive and destructive interference and other wave-related phenomena.

In this book, we will discuss only those methods applicable to very small randomly oriented particles (Rayleigh theory) or to spheres of arbitrary size (Mie theory). Fortunately, a great many atmospheric particles, from molecules to haze droplets to cloud droplets to rain drops to hailstones, are reasonable (though not always perfect) candidates for one or both of these methods, so we can cover a fair amount of ground.

12.1.2 Relevant Properties

As already mentioned, the relationship between the size of a particle and the wavelength of the radiation of interest is of crucial importance to particle's optical properties as well as to the choice of a suitable method for calculating those properties. We therefore define the nondimensional *size parameter* as

$$\boxed{x \equiv \frac{2\pi r}{\lambda}}, \tag{12.1}$$

where r is the radius of a spherical particle. In the case of nonspherical particles, r might represent the radius of a sphere having the same volume or surface area, depending on the context.

[3]Even for large particles, geometric optics gives results that are seemingly at odds with exact theories. The discrepancy is due to the inability of ray tracing alone to account for subtle bending of light waves passing *near* the particle. However, because the bending is slight, it is often acceptable to treat this radiation as if it had never been scattered at all, in which case the geometric optics approximation yields perfectly acceptable results.

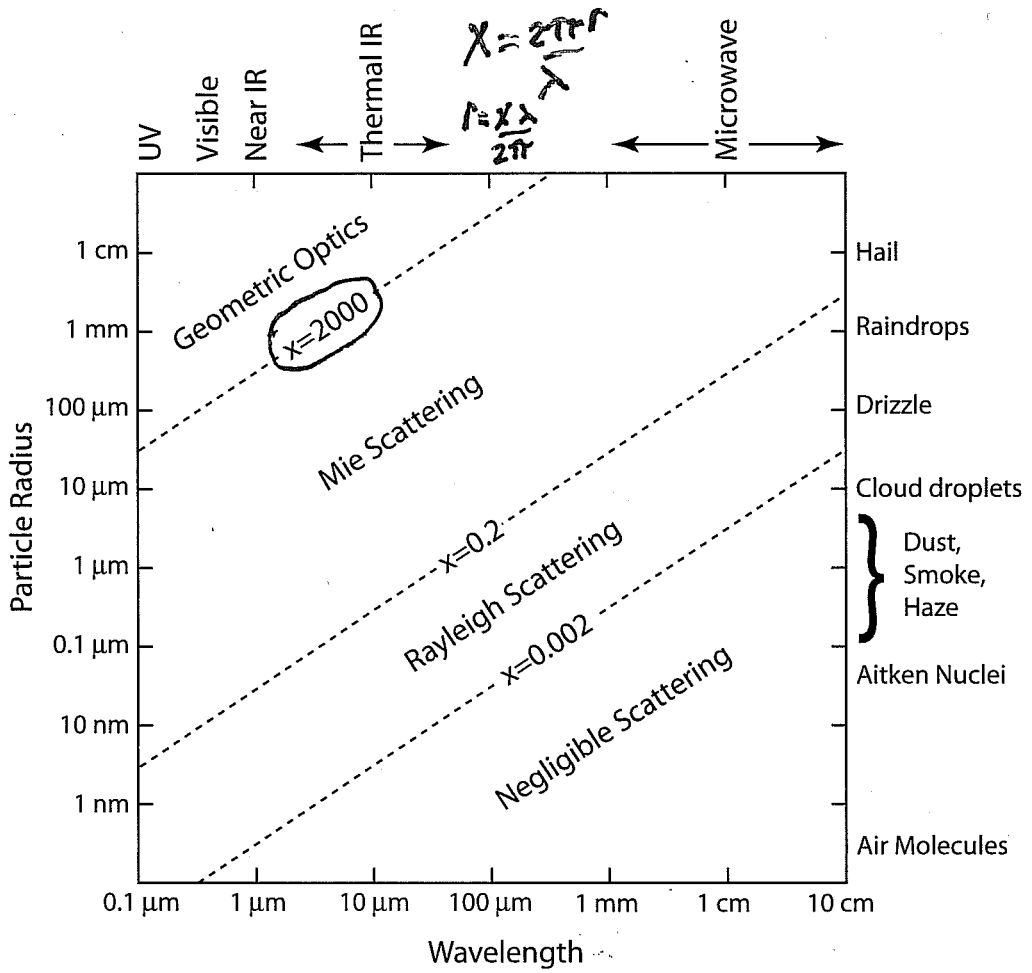

Fig. 12.1: Relationship between particle size, radiation wavelength and scattering behavior for atmospheric particles. Diagonal dashed lines represent rough boundaries between scattering regimes.

Given the value of x, one can immediately determine whether scattering by the particle is likely to be significant and, if so, which broad *scattering regime* — Rayleigh, Mie, or geometric optics — is most applicable. Figure 12.1 shows how various combinations of particle type and EM wavelength relate to these regimes.

Another key property is the relative index of refraction m, which

was defined in (4.19) as

$$\boxed{m \equiv \frac{N_2}{N_1},}$$

where N_2 and N_1 are complex refractive indices of the particle and the surrounding medium, respectively. At the risk of slightly oversimplifying, the real part $n_r = \Re(N)$ governs the phase speed of propagation of a wave within the material and the imaginary part $n_i = \Im(N)$ governs absorption. N_1 is usually taken to be equal to one for particles suspended in air, so that $m \approx N_2$. N_2 depends on both the composition of the particle and on the wavelength. The dependence of the refractive index of water and ice on wavelength was shown in Fig. 4.1.

Finally, the *shape* of a particle may potentially play a large role in determining its radiative properties. It is convenient, and therefore common, to assume that particles are spheres for radiative purposes, even when this assumption is not entirely appropriate. Ice crystals, snowflakes, and solid-phase aerosols (e.g., soot) are good examples of particles that are far from spherical and therefore should really not be treated as such, at least not without prominently posted disclaimers. Unfortunately, computational methods appropriate for nonspherical particles are far more difficult to work with and have only recently come into common use with the advent of fast computers. We will not consider them here.

12.2 Scattering by Small Particles

12.2.1 Dipole Radiation

When a particle is sufficiently small relative to the wavelength — i.e., $|m|x \ll 1$ — every part of the particle simultaneously experiences the same externally imposed oscillating electric field. The response of the particle to the electric field is to become partially polarized. That is, there is a small displacement of positive charge within the particle in the direction of the electric field vector, while there is a displacement of negative charge in the opposite direction. In short, it becomes an electric *dipole*, with induced *dipole moment*

$\vec{\mathbf{p}}$. The physical dimensions of $\vec{\mathbf{p}}$ are charge times distance, which can be interpreted as the net amount of charge Q displaced times an effective displacement $\vec{\mathbf{x}}$.

For most particles of interest to us, the dipole moment of a small spherical particle is proportional to the strength of the external electric field:

$$\vec{\mathbf{p}} = \alpha \vec{\mathbf{E}}_0 \exp(i\omega t) , \tag{12.2}$$

where α is called the *polarizability* of the particle. It depends on the composition and the size of the particle, as well as on the frequency $\omega = 2\pi\nu$ of the incident wave. Note that α may be complex. Any nonzero imaginary part implies a phase difference between the real part of $\vec{\mathbf{p}}$ and the real part of $\vec{\mathbf{E}}$.

In summary, we have an oscillating dipole whose strength and orientation fluctuates in lockstep with the electric field due to the incident wave. But an oscillating dipole produces its own oscillating electric field, and these oscillations propagate outward at the speed of light. This is of course the origin of the scattered radiation.

Now imagine that the incident wave is traveling in direction $\hat{\mathbf{\Omega}}$ and you are positioned at a large distance $R \gg r$ from the dipole, in direction $\hat{\mathbf{\Omega}}'$. There are several facts we can jot down that will aid us in visualizing the relationship between the scattered wave at our location and the incident wave:

1. We know that in any EM wave, the electric field vector is perpendicular to the direction of propagation $\hat{\mathbf{\Omega}}$.

2. We are assuming here that $\vec{\mathbf{p}}$ is aligned with the electric field $\vec{\mathbf{E}}_0$ of the incident wave,[4] so $\vec{\mathbf{p}}$ is also perpendicular to $\hat{\mathbf{\Omega}}$.

3. Because of the symmetry of the charge distribution in the dipole, the electric field vector $\vec{\mathbf{E}}_{\text{scat}}$ of the scattered wave at any location must lie in the plane that contains both $\vec{\mathbf{p}}$ and $\hat{\mathbf{\Omega}}'$.

4. The *strength* of the electric field at your location is proportional to the *projection* of $\vec{\mathbf{p}}$ as seen from your direction. Specifically,

[4] In other words, we are assuming that the polarizability α is a *scalar* rather than a 3×3 *tensor* which would alter the direction of $\vec{\mathbf{p}}$ relative to $\vec{\mathbf{E}}_0$. This is always valid for spherical particles composed of an electrically isotropic substance like water.

$\vec{\mathbf{E}}_{\text{scat}}$ is zero if you are viewing the dipole "end on" and it is a maximum (for a given distance) when you are viewing it at right angles. We can put this in mathematical terms by saying that $\vec{\mathbf{E}}_{\text{scat}} \propto \sin\gamma$, where γ is the angle between $\vec{\mathbf{E}}_0$ (using Fact 2, above) and the scattered direction $\hat{\mathbf{\Omega}}'$.

5. Less obvious, but equally important, is that the power radiated by the dipole is proportional to the *acceleration* of the electric charge in the dipole. That is to say, a stationary dipole will create a static electric field but no propagating EM wave, and it will therefore radiate no energy. A vibrating dipole, on the other hand, induces a vibrating electric field (and therefore an outward propagating EM wave) whose amplitude is proportional to the *square* of the frequency of the vibration.

Facts 4 and 5 together, combined with (12.2), give us the following proportionality:

$$|\vec{\mathbf{E}}_{\text{scat}}| \propto \frac{\partial^2 \vec{\mathbf{p}}}{\partial t^2} \sin\gamma \propto \omega^2 \sin\gamma \,. \tag{12.3}$$

As discussed in section 2.5, the *power per unit area*, and therefore the intensity I, is proportional to the *square* of the electric field amplitude. Therefore, the scattered intensity is given by the following proportionality:

$$I \propto \omega^4 \sin^2\gamma \,. \tag{12.4}$$

We now want to recast the above proportionality in terms of the scattering angles Θ and Φ, where Θ is the angle between $\hat{\mathbf{\Omega}}$ and $\hat{\mathbf{\Omega}}'$, and Φ is the polar angle about $\hat{\mathbf{\Omega}}$ measured from an arbitrary starting point.

For convenience, we let the direction of incidence $\hat{\mathbf{\Omega}}$ coincide with the x-axis, and the incident electric field vector $\vec{\mathbf{E}}_0$ be aligned with the z-axis, consistent with Fact 2, above. We can then expand $\hat{\mathbf{\Omega}}$ and $\hat{\mathbf{\Omega}}'$ in Cartesian coordinates as follows:

$$\hat{\mathbf{\Omega}} = (1,0,0) \,, \tag{12.5}$$

$$\hat{\mathbf{\Omega}}' = (\cos\Theta, \sin\Theta\sin\Phi, \sin\Theta\cos\Phi) \,. \tag{12.6}$$

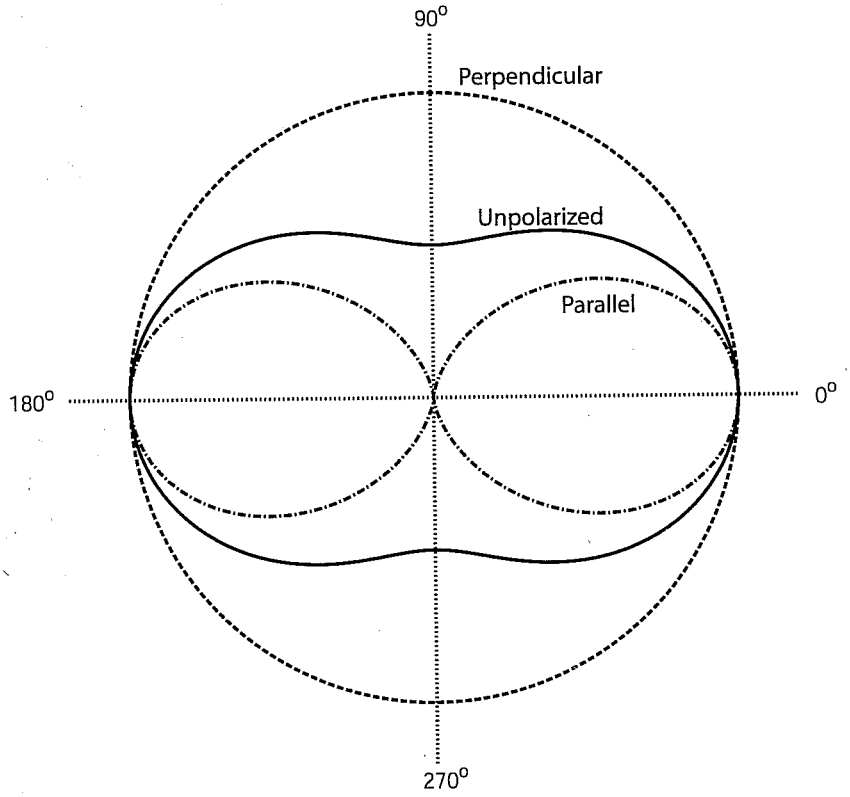

Fig. 12.2: Polar plot of the phase function for scattering by small particles (Rayleigh scattering). The outermost curve (dashed) represents the scattered intensity for directions $\hat{\mathbf{\Omega}}'$ lying in a plane *perpendicular* to the electric field vector of the incident wave. The innermost curve (dot-dashed) corresponds to directions lying in a plane *parallel* to the electric field vector. The solid curve represents the scattered intensity for unpolarized incident radiation, as given by (12.10).

This allows us to write

$$\begin{aligned} \cos\gamma &= \hat{\mathbf{z}} \cdot \hat{\mathbf{\Omega}}' \\ &= (0,0,1) \cdot \hat{\mathbf{\Omega}}' \\ &= \sin\Theta\cos\Phi\,, \end{aligned} \tag{12.7}$$

and

$$\sin^2\gamma = 1 - \cos^2\gamma \quad = 1 - \sin^2\Theta\cos^2\Phi\,. \tag{12.8}$$

Substituting into (12.4) gives

$$I \propto \omega^4(1 - \sin^2\Theta\cos^2\Phi)\,. \tag{12.9}$$

The above equation contains all of the essential features of what we will henceforth refer to as *Rayleigh scattering*. Before we continue, let's take a moment to interpret this result:

- The intensity of scattered radiation is proportional to the *fourth power* of the frequency of the incident radiation, assuming that the polarizability α is not a strong function of frequency (this may or may not be true for any given particle). You should mentally file this piece of information; we will return to it later.

- For Φ equal to either 90° or 270° — in other words, for any scattered ray lying in the plane perpendicular to $\vec{E}_0$, the scattered intensity is both constant and at its maximum value, irrespective of Θ (the outermost curve in Fig. 12.2).

- For Φ equal to either 0° or 180° *and* $\Theta = 90°$ — in other words, for either of the two directions along the axis of the dipole — the scattered intensity is zero (see the innermost curve in Fig. 12.2).

12.2.2 The Rayleigh Phase Function

The complete shape of the Rayleigh phase function for polarized incident radiation is shown in the top two panels of Fig. 12.3. For unpolarized incident radiation, the phase function $p(\Theta)$ is obtained by averaging (12.9) over Φ and normalizing according to (11.7) to get

$$\boxed{p(\Theta) = \frac{3}{4}(1 + \cos^2\Theta)\ .} \qquad (12.10)$$

The above expression is the one that we normally regard as describing the scattering phase function of very small particles. It is depicted as the solid curve in Fig. 12.2 and in the bottom panel of Fig. 12.3.

Problem 12.1: Verify the derivation of (12.10) from (12.9).

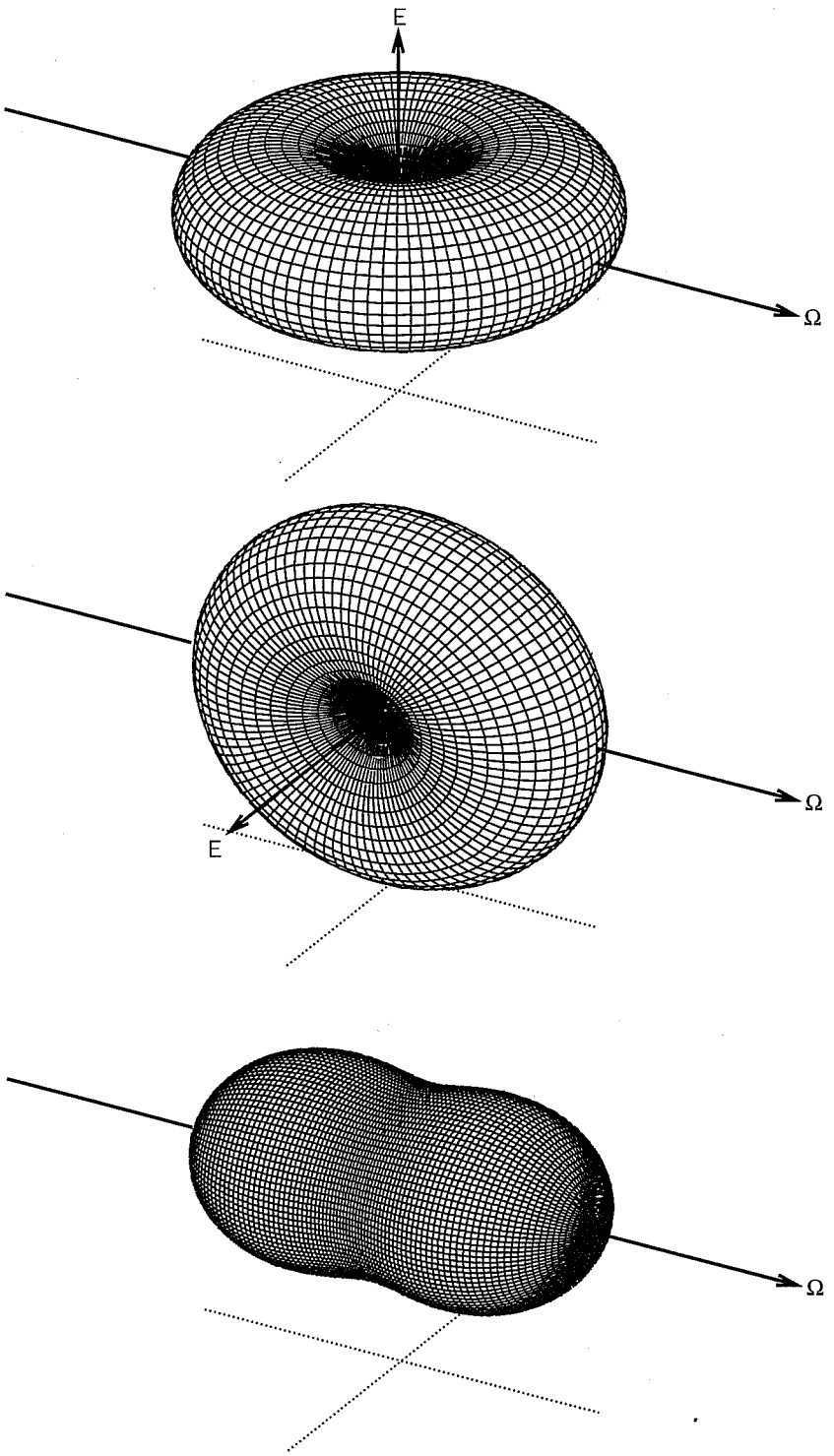

Fig. 12.3: Three-dimensional rendering of the Rayleigh phase function. The vector Ω indicates the direction of the incident radiation. The vector E indicates the orientation of the electric field vector in the incident wave. Top: Incident radiation is vertically polarized. Middle: Incident radiation is horizontally polarized. Bottom: Incident radiation is unpolarized.

Problem 12.2: From (12.10), show that the asymmetry parameter g for Rayleigh scattering is zero.

$$g \equiv \frac{1}{4\pi} \int_{4\pi} p(\cos\Theta) \cos\Theta \, d\omega$$

Solid angle

12.2.3 Polarization

Equation (12.10) assumes that the incident radiation is unpolarized. But note that even if unpolarized light is incident on the particle, *the scattered light will, in general, be polarized.* You can convince yourself of this by imagining yourself positioned in the direction indicated by the ray labeled E in the *middle* panel of Fig. 12.3, which is to say, at a 90° angle to a horizontal beam of incident radiation (e.g., from the setting sun). At this position, you will observe no scattering of the horizontally polarized component of the incident radiation. You *will*, however, observe the maximum amount of scattering of the vertically polarized component of the incident radiation. Moreover, the scattered radiation in the latter case will itself be vertically polarized.

In short, viewing in any direction at 90° to the incident beam, you will see scattered radiation that is completely polarized. At most other angles, the scattered radiation is partially polarized, because neither component is zero. Only in the forward direction ($\Theta = 0°$) or the backward direction ($\Theta = 180°$), is the degree of scattering the same regardless of the polarization of the incident radiation; hence, unpolarized incident radiation gives rise to unpolarized scattered radiation in these two directions. In general, the degree of polarization of Rayleigh-scattered radiation is given by

$$\boxed{P = \frac{1 - \cos^2\Theta}{1 + \cos^2\Theta}} \,. \qquad (12.11)$$

Radiation from the cloud- and haze-free sky is dominated by Rayleigh scattering by air molecules. According to the above equation, skylight will be unpolarized when looking directly toward or away from the sun, and 100% polarized when viewing the sky at a 90° angle from the sun.

In reality, the inevitable presence of aerosols, which are much larger than molecules and don't satisfy the Rayleigh criterion, reduces the polarization somewhat. Also, multiple scattering, which is weak but not negligible in this instance, further reduces the polarization slightly.

Nevertheless, wearing a pair of polarized sunglasses, you can easily verify the above effect by viewing a portion of the blue sky at right angles from the sun and rotating the sunglasses (or your head) about the line-of-sight. The sky will appear darker or lighter, depending on whether the sunglasses transmit or block the polarized radiation. The bluer the sky (and therefore the less haze present) the more pronounced the effect will be.

12.2.4 Scattering and Absorption Efficiencies

We were able to infer the scattering phase function for small particles based on relatively simple handwaving arguments. Let's now turn to the question of how *much* radiation a small particle scatters and/or absorbs. While it is possible to obtain this information directly based on the dipole model we developed above (see BH83, section 5.2), the complete derivation requires more space and explanation than seems warranted at this introductory level. Among other things, it would be necessary to explain the relationship between the (relative) complex index of refraction m of the particle and its polarizability α, as well as to show how the imaginary part of α bears on absorption of the incident electromagnetic wave by the particle.

An alternate way of getting at the same information is to take the general Mie solutions for spheres of arbitrary size, which I will briefly discuss in section 12.3, and find limiting expressions for $x \ll 1$. Specifically, you rewrite the solutions as power series in x and discard all but the first few terms. Here, I will give you the essential results without going through the derivations (see BH83, section 5.1).

General Relationships

To terms of order x^4, the extinction and scattering efficiencies, respectively, of a small spherical particle are

$$Q_e = 4x\Im\left\{\frac{m^2-1}{m^2+2}\left[1+\frac{x^2}{15}\left(\frac{m^2-1}{m^2+2}\right)\frac{m^4+27m^2+38}{2m^2+3}\right]\right\} + \frac{8}{3}x^4\Re\left\{\left(\frac{m^2-1}{m^2+2}\right)^2\right\}, \quad (12.12)$$

and

$$\boxed{Q_s = \frac{8}{3}x^4\left|\frac{m^2-1}{m^2+2}\right|^2 .} \quad (12.13)$$

The absorption efficiency is then $Q_a = Q_e - Q_s$. For sufficiently small x (see BH83, p. 136 for details), Q_a simplifies to

$$\boxed{Q_a = 4x\Im\left\{\frac{m^2-1}{m^2+2}\right\} .} \quad (12.14)$$

We see that the absorption efficiency Q_a is proportional to x, while the scattering efficiency Q_s is proportional to x^4. It follows that, for sufficiently small x, and assuming that m has a nonzero imaginary part,

$$\boxed{Q_s \ll Q_a \approx Q_e ,} \quad (12.15)$$

and the single scatter albedo

$$\boxed{\tilde{\omega} \equiv \frac{Q_s}{Q_e} \propto x^3 .} \quad (12.16)$$

The above relationships have a number of important practical implications for atmospheric radiation and remote sensing. We will highlight a few of these here.

Scattering Cross-Section

First of all, if we assume that we're in a part of the spectrum where m for our particle varies slowly with wavelength, then according to (12.13) the scattering efficiency Q_s of a particle in the Rayleigh limit is proportional to x^4, which is in turn proportional to $(r/\lambda)^4$ or, equivalently, to $(r\nu)^4$. [Recall that we already saw this proportionality in (12.9), since $\omega \equiv 2\pi\nu$.] The scattering *cross-section* σ_s, which is what actually determines how much radiation is scattered, is of course the product of Q_s with the particle cross-sectional area πr^2, so that

$$\boxed{\sigma_s \propto \frac{r^6}{\lambda^4}\,.} \qquad \text{Rayleigh Scattering Cross section} \qquad (12.17)$$

This proportionality is well worth memorizing, as long as you also remember that it's only valid in the Rayleigh regime — i.e., for $x \ll 1$.

Single Scatter Albedo

The second relationship worth commenting on is (12.16), which tells us that the single scatter albedo for small particles goes with x^3. Of course this is only true for particles that are at least slightly absorbing; if the imaginary part of m is zero, then $\tilde{\omega} = 1$ no matter how small x.

What this means in practice is that for sufficiently small x you can pretty much forget about scattering and focus instead on just the absorption properties of the particles. This limiting behavior arises in at least two important cases: (1) molecular absorption (but not scattering) of thermal infrared radiation by atmsospheric gases (see Chapter 9), and (2) absorption (but not scattering) of microwave radiation by cloud droplets.

Mass Absorption Coefficient

Not only can you forget about *scattering* in the limit of small x, but a surprisingly convenient fact emerges concerning *absorption* by particles in this limit. Recall that the mass absorption coefficient k_a of a substance is defined as its absorption cross-section per unit mass.

For a spherical particle of radius r and density ρ, we can write

$$k_a = \frac{Q_a \pi r^2}{\rho(4/3)\pi r^3} = \frac{3Q_a}{4\rho r} . \tag{12.18}$$

Substituting (12.14) and (12.1), we have

$$k_a = \frac{6\pi}{\rho\lambda} \Im\left\{\frac{m^2-1}{m^2+2}\right\} . \tag{12.19}$$

Approximate for soot and visible

Note that *there is no dependence here on the particle radius r*!

Imagine a volume V of air containing a number of spherical particles (e.g., cloud droplets) which may be of various sizes but which are in any case all much smaller than the wavelength of interest. We can write the volume absorption ($\approx$ extinction) coefficient (dimensions of inverse length) in terms of the sum of the particles' individual absorption cross-sections σ as follows:

$$\beta_a = \frac{1}{V}\sum_i \sigma_i . \tag{12.20}$$

But $\sigma_i = k_a M_i$, where M_i is the mass of the droplet, so we have

$$\beta_a = \frac{1}{V}\sum_i k_a M_i = k_a \frac{1}{V}\sum_i M_i \tag{12.21}$$

or, quite simply,

$$\boxed{\beta_a = k_a \rho ,} \tag{12.22}$$

where ρ is just the combined mass of the substance (e.g., cloud water) per unit volume of air. We therefore conclude that *for radiation passing through a cloud of sufficiently small absorbing particles, the total absorption is equal to* k_a [as given by (12.19)] *times the total mass path, regardless of the exact sizes of the constituent particles.*

Summary

Let us conclude this section by summarizing some **key facts** about scattering and absorption in the Rayleigh regime:

1. If you have a particle of fixed size and expose it to radiation with two different wavelengths $\lambda_1 < \lambda_2$, then it will scatter the shorter wavelength λ_1 more strongly by a factor of $(\lambda_2/\lambda_1)^4$.

2. If you have radiation of a fixed wavelength λ and use it to illuminate two particles of radius $r_1 < r_2$, the larger particle will scatter the radiation more strongly by a factor $(r_2/r_1)^6$.

3. For sufficiently small particles with complex (not pure real) refractive index m, scattering is negligible and absorption is proportional to mass path only, irrespective of particle size. In this limit, a cloud behaves radiatively like an absorbing gas rather than a collection of discrete scatterers.

The first of these facts is directly responsible for the blue sky and the reddish setting sun. The second fact is of central importance to weather radar. The third is relevant to microwave remote sensing of cloud water. We will revisit each of these topics in the Applications section at the end of this chapter.

12.3 Scattering by Spheres — Mie Theory

A brief outline of Mie theory for scattering and absorption by homogeneous spheres of arbitrary size parameter x and relative index of refraction m is given by S94 (pp. 235–243). Full derivations are given by BH83 (pp. 82–107) and L02 Section 5.2. In a nutshell, the Maxwell equations are used to derive a wave equation for electromagnetic radiation in three dimensional space, and these are expressed in spherical polar coordinates (r, ϕ, Θ), with appropriate boundary conditions at the surface of the sphere. The result is a separable partial differential equation, the solution of which is expressed as an infinite series of products of orthogonal basis functions, including sines and cosines (for the dependence on ϕ), spherical Bessel functions (for the dependence on r), and associated Legendre polynomials (for the dependence on $\cos\Theta$).

If you have already had a course in partial differential equations, then that last sentence will be at least vaguely intelligible. The bottom line is that the extinction and scattering efficiencies of a sphere

may be written as

$$Q_e = \frac{2}{x^2}\sum_{n=1}^{\infty}(2n+1)\Re(a_n + b_n)\,, \tag{12.23}$$

$$Q_s = \frac{2}{x^2}\sum_{n=1}^{\infty}(2n+1)(|a_n|^2 + |b_n|^2)\,, \tag{12.24}$$

where the coefficients a_n and b_n are referred to as Mie scattering coefficients and are functions of x and m. The mathematical form of these coefficients is not particularly informative to the untrained eye, so they will not be reproduced here.

Similar summations are used to describe the wave scattering amplitudes as a function of scattering angle Θ. These are used to obtain expressions for the elements of the 4×4 scattering phase matrix $P_{ij}(\Theta)$ (see 11.2.2). The P_{11} element of this matrix is the same as our scalar phase function $p(\Theta)$ for unpolarized incident light.

As a practical matter, one cannot actually compute an infinite sum; therefore it is always necessary to truncate the series and keep only enough terms to yield a sufficiently accurate approximation. Generally speaking, the required number of terms N is a little larger than x; the criterion developed by BH83 based on extensive testing is that N should be the integer closest to $x + 4x^{1/3} + 2$. For a typical cloud droplet of 10 μm radius and a visible wavelength of 0.5 μm, the size parameter $x \approx 120$; thus the number of terms required in the summation is 127.

For much larger particles (e.g. raindrops in the visible band, with $x \sim 10^4$ or more) the number of terms that must be retained is rather large. Although the computer time required to evaluate these terms is no longer a huge issue for most applications, numerical precision begins to suffer due to the accumulation of roundoff error. There are therefore practical limits to the size of a sphere whose properties can be evaluated using Mie theory. Geometric optics (or ray tracing; see Section 4.3.1) becomes the preferred method in such cases.

12.3.1 Extinction Efficiency for Nonabsorbing Sphere

Figure 12.4 depicts the extinction efficiency Q_e as a function of x for a sphere with $m = 1.33$. This is a representative value for water in

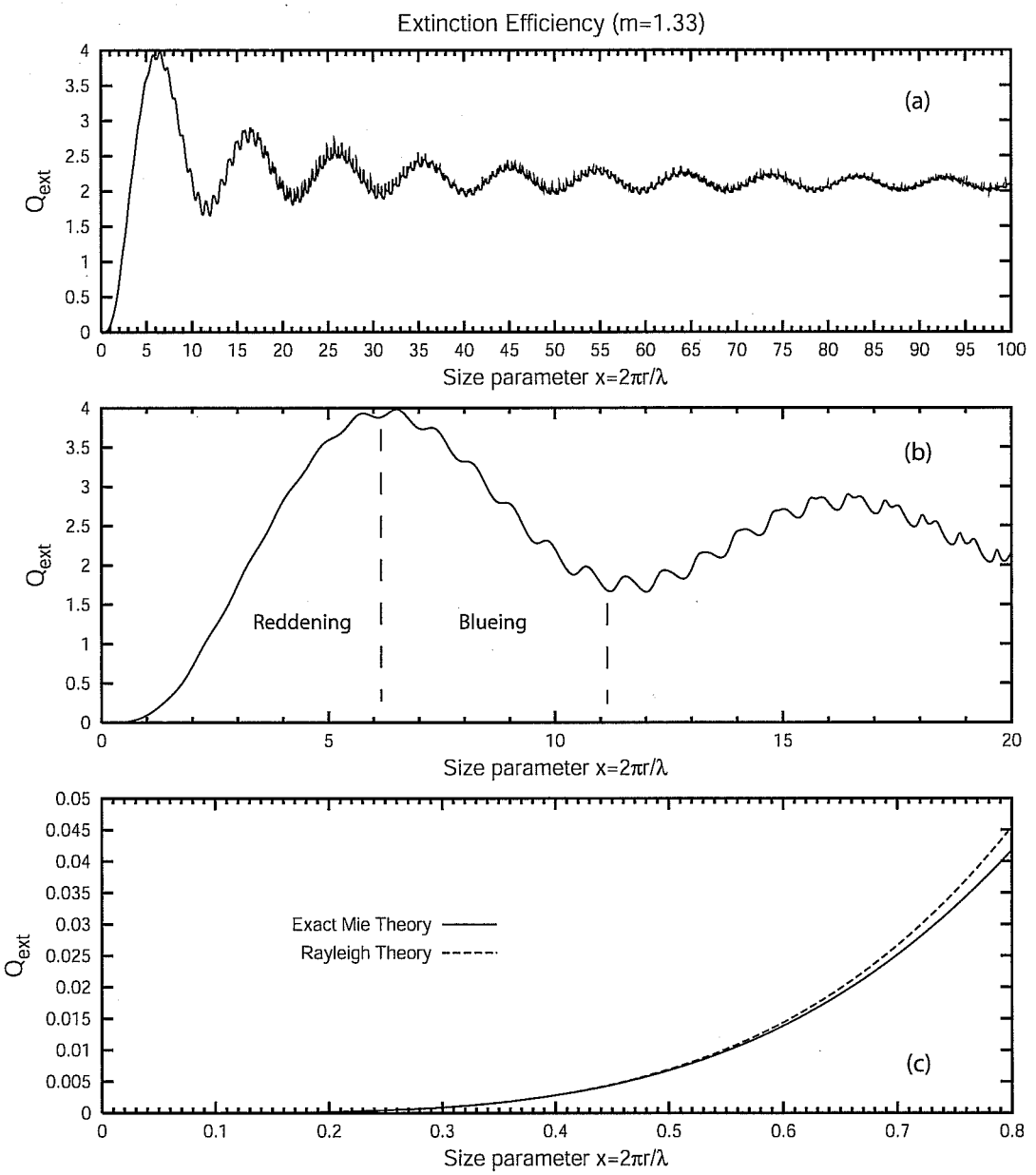

Fig. 12.4: The extinction efficiency Q_e as a function of size parameter x for a nonabsorbing sphere with $m = 1.33$, for various ranges of x. (a) "Big picture" view, showing that $Q_e \to 2$ as $x \to \infty$. (b) Detail for $x < 20$, with examples of subranges for which extinction increases with x (reddening) or decreases with x (blueing). (c) Detail for $x < 0.8$, comparing the Rayleigh (small particle) approximation and exact Mie theory.

the visible band. Note that no imaginary part is assumed here, so the droplet is nonabsorbing ($\tilde{\omega} = 1$) for all x.

The top panel (Fig. 12.4a) shows the typical behavior of Q_e over a wide range of x. It starts out at zero for $x = 0$ and rises monotonically up to about $x = 6$, where Q_e achieves a maximum value

of about 4. In other words, for this value of x, the droplet scatters four times as much radiation as one might surmise from its cross-sectional area alone! Thereafter, it exhibits an ever-dampening oscillation about a mean value of 2, which is the limiting value of Q_e for large x (recall that we already exploited this behavior in section 7.2.3).

At the other end of the range, we have the opportunity to compare $Q_e (= Q_s)$ computed using the exact Mie theory with that obtained for the small-particle (Rayleigh) limit (Fig. 12.4c). We can see that the agreement is quite good up to about $x = 0.6$. Beyond that point, Q_e increases less rapidly than the x^4 dependence predicted by (12.13).

Reddening/Blueing

Let's now zoom in on the first couple of big wiggles in the curve (Fig. 12.4b). Let's further assume for the moment that r is fixed, so that variations in x are due to variations in the wavelength λ, not particle size — that is, increasing x implies decreasing λ, and vice versa. Despite allowing the wavelength to vary, we will pretend (somewhat unrealistically) that m also remains approximately constant, so that our Q_e curves are still valid.

With the above assumptions in mind, we find that in the region $0 < x < 6$, Q_e increases with x and therefore decreases with wavelength. This means that for radiation passing through a cloud of our fixed-size particles, the shorter wavelengths will be attenuated more strongly than the longer wavelengths. This phenomenon is known as *reddening*, and is responsible for the reddish color of the setting sun. In fact, we already found a similar phenomenon in connection with Rayleigh scattering in the previous section; those findings applied to particles with $x \ll 1$, which is of course a small portion of the range of x we are looking at right now.

For x between 6 and 11, on the other hand, extinction is stronger for longer wavelengths than for shorter, giving rise to *blueing* of the radiation passing through our particles. Blueing of sunlight or moonlight is only very rarely observed; it would require an unusual distribution of aerosol sizes in order for the blueing effect to dominate over the usual reddening by both air molecules and smaller

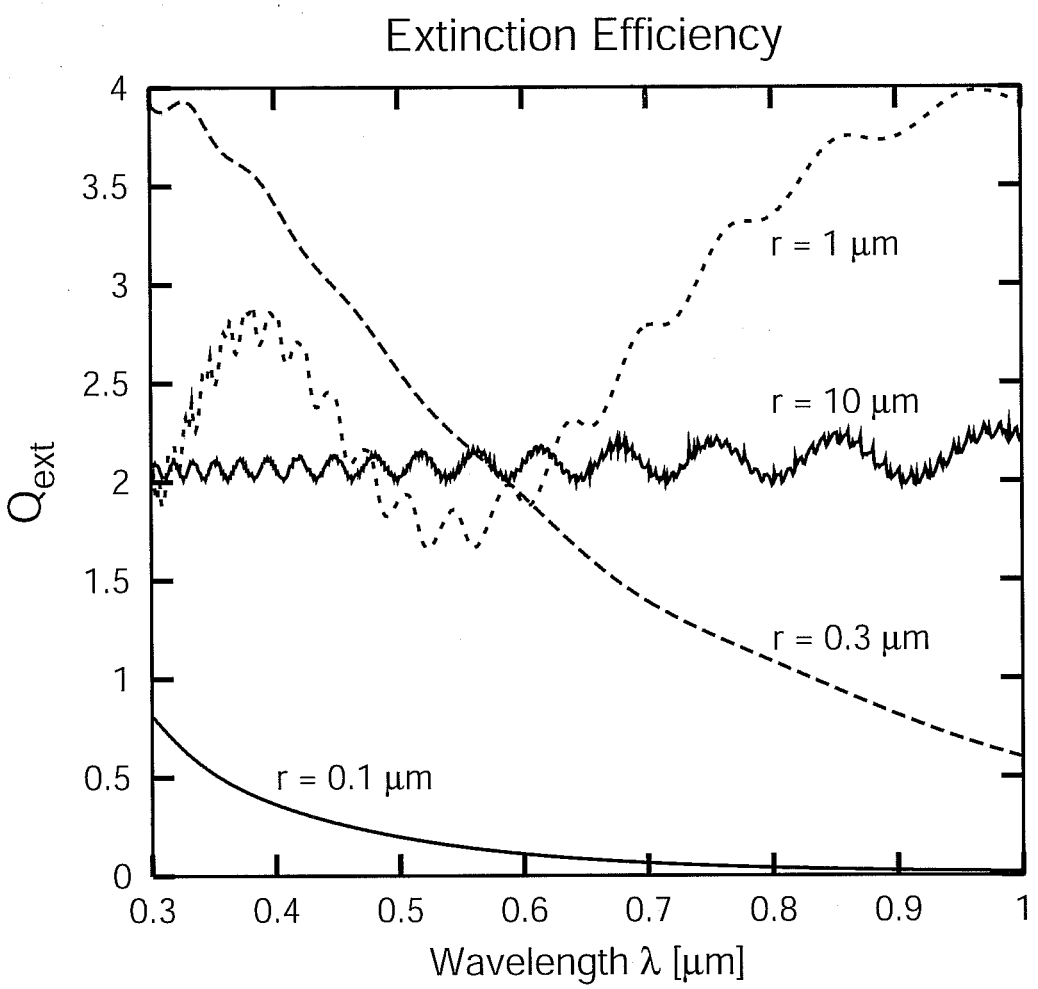

Fig. 12.5: The extinction efficiency as a function of wavelength for water droplets of the indicated sizes.

aerosols.[5]

Problem 12.3: Visible radiation spans the wavelength range from 0.4 μm to 0.7 μm. Assuming that atmospheric aerosols have approximately the same refractive index m as that used to produce Fig. 12.4b, determine the range of aerosol radii that would give rise to blueing.

We can look at the above phenomenon from a slightly different (and more realistic) perspective by plotting the extinction efficiency

[5]Large volcanic eruptions occasionally inject matter into the stratosphere that coalesces into aerosols of fairly uniform size; on rare occasions these may have a size that leads to blueing of visible light. Some authors have suggested that such rare events gave rise to the phrase "once in a blue moon."

versus wavelength for selected water droplet radii, as in Fig. 12.5. For droplet radii of 0.1 and 0.3 μm, which are characteristic of small haze droplets, extinction is a strong function of wavelength, with short wavelengths (e.g., UV-A, violet, blue) being extinguished far more strongly than longer wavelengths (red, near IR). This is again the classic reddening behavior that we observe on a hazy day, especially when the sun is low in the sky.

At an intermediate radius of 1 μm, the extinction behavior is more complex. Near infrared wavelengths are fairly strongly attenuated, violet light (near 0.4 μm) and red light (near 0.7 μm) is attenuated slightly less strongly, and there is a pronounced minimum in extinction between 0.5 and 0.6 μm. We can conclude that if the aerosol population of the atmosphere consisted primarily of droplets of 1 μm radius, the setting sun would take on a rather unnatural greenish hue![6]

The largest radius for which Q_e is plotted in Fig. 12.5 is 10 μm, which is a typical radius for ordinary cloud droplets. Over the entire range of wavelength plotted, $Q_e \approx 2$. The lack of strong wavelength dependence is why the color of sunlight passing through thin clouds is not noticeably altered by the encounter. Even the obvious wiggles seen on this curve are actually irrelevant in practice, because cloud droplets never have exactly one size but rather are distributed over a fairly broad range of sizes. Even a fairly small 10% variability in droplet size would be enough to average away most of the wiggle structure in the Q_e curve.

12.3.2 Extinction and Scattering by Absorbing Spheres

Let's now broaden our perspective in the following two ways: (1) we will allow the imaginary part of m to be nonzero, and (2) we will look at not only Q_e but also the absorption efficiency Q_a, the single scatter albedo $\tilde{\omega}$, and the scattering asymmetry parameter g. Representative results are shown in Fig. 12.6. Based on these plots

[6] It is tempting, though probably futile, to speculate on a possible role for 1 μm haze or cloud droplets in the sickly greenish light that is observed to accompany some severe thunderstorms. Various other physical mechanisms have been proposed; as of this writing none has been widely embraced as *the* definitive explanation for green thunderstorms, partly because of the scarcity of direct measurements that could be used to test the various theories.

(Yes! Near sunset, reddening (blue removed) by Rayleigh

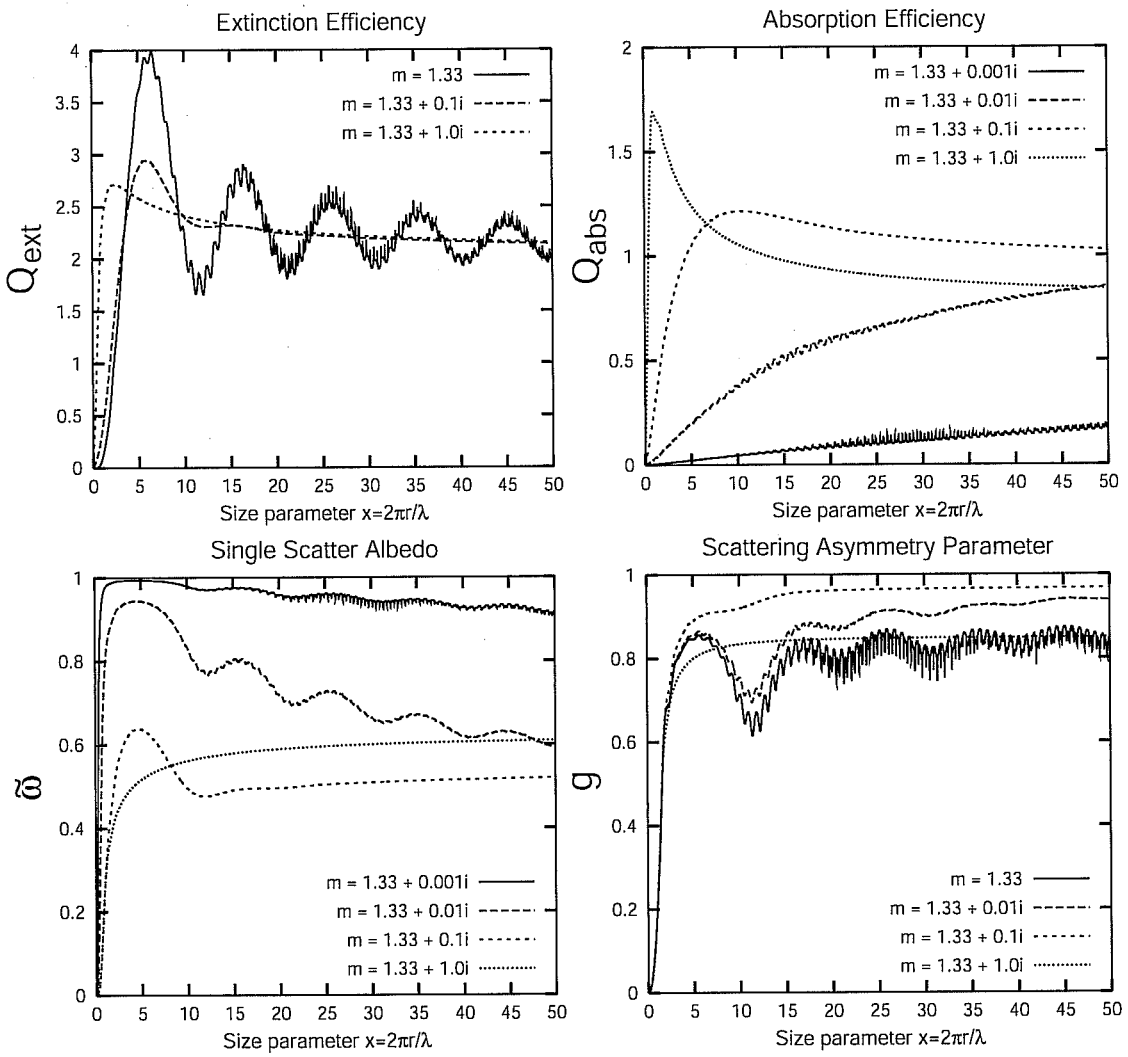

Fig. 12.6: Key optical properties of spheres as functions of x, for varying values of the imaginary part of m.

we can make the following general statements:

- Increasing absorption by the particle material (by increasing the imaginary part of m) has the effect of suppressing the wiggles in the curve of Q_e. Apart from that change, the curves are similar, all having a limiting value of approximately 2 for large x.

- In the limit as x goes to zero, the single scatter albedo also goes to zero, as predicted by (12.16). The sole exception is if $\Im(m) = 0$ (not shown), in which case $\tilde{\omega} = 1$ regardless of x.

- For $x > 10$, there is no completely predictable relationship

between $\Im(m)$ and either Q_a or $\tilde{\omega}$. The absorption tends to increase with small increases in $\Im(m)$, as you might expect, but the trend reverses when $\Im(m)$ is of order one — particles with large $\Im(m)$ scatter *more* effectively than those with smaller $\Im(m)$.

- For $\Im(m) = 0$, there is considerable fine ripple structure in the curves for both Q_e and g. The presence of even slight absorption (e.g., the case $m = 1.33 + 0.001i$) pretty much eliminates these ripples. But even for nonabsorbing particles, these fine ripples tend to be unimportant. This is because you never have particles all having the same exact value of x but rather a mix of particles of various sizes. When combining the contributions from various sizes, the small ripples quickly average away.

- For $x = 0$, the asymmetry parameter g is also zero, as expected for Rayleigh scattering. As x increases, g very rapidly increases as well, plateauing somewhere in the range from about 0.8 and 0.95.

Forward Scattering

The last item is worthy of particular attention. It indicates that *particles comparable to or larger than the wavelength tend to strongly forward scatter*, as contrasted with the case that $x \ll 1$, for which the backward and forward scattered components are about equal. It turns out that *this observation is generally applicable not only to spheres but to particles of all types and shapes.* This behavior is due to constructive interference in the forward direction by waves scattered by different parts of the particle, as discussed for example by S94 (Section 5.2.1).

12.3.3 Scattering Phase Function

The forward-scattering properties of larger particles becomes even more apparent as we turn our attention to the scattering phase function $p(\Theta)$ of our spheres, as depicted for example in Fig. 12.7.

For $x = 0.1$ (bottom), we have the classical Rayleigh phase function, which is symmetric in the forward and backward directions.

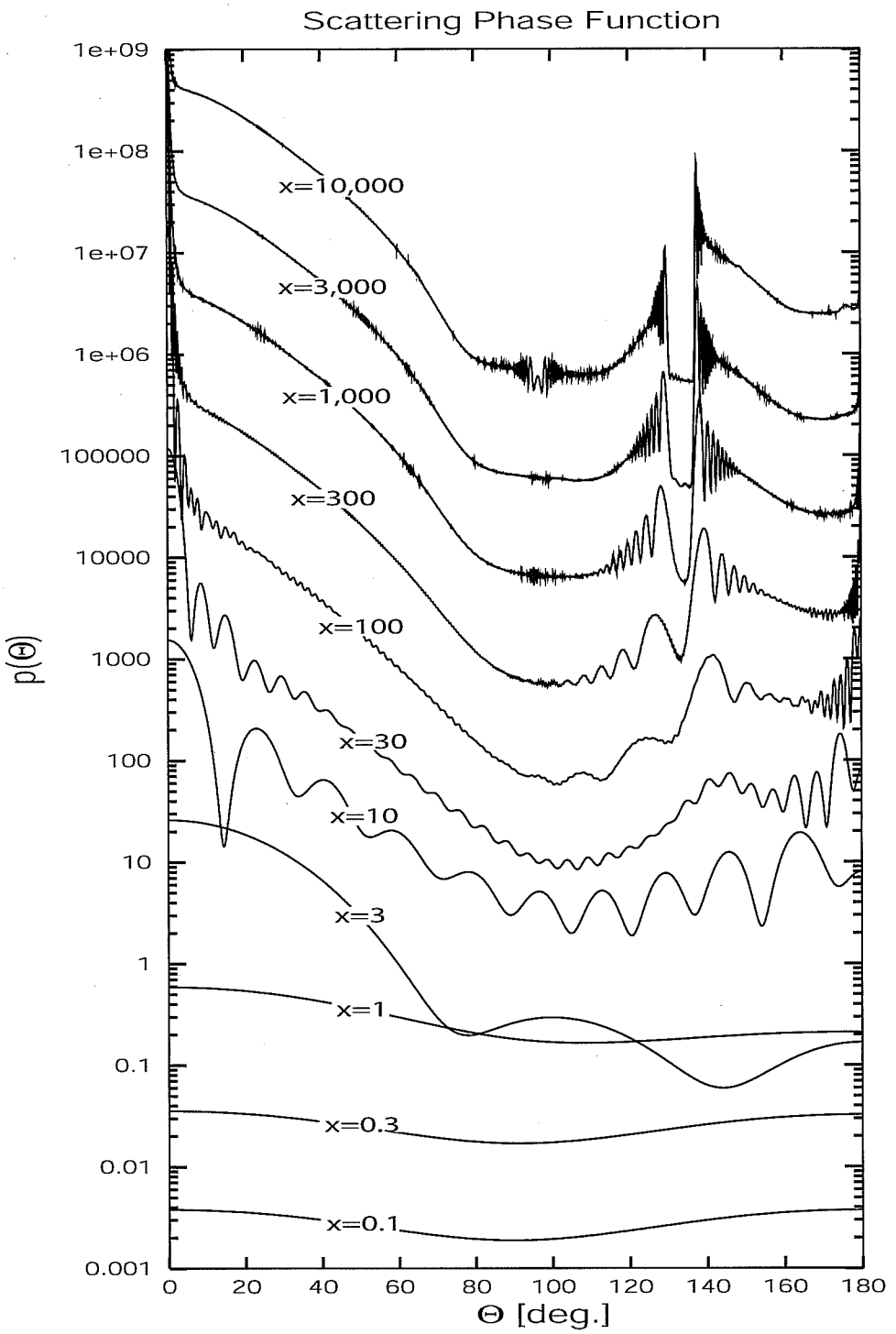

Fig. 12.7: Plots of Mie-derived phase functions $p(\Theta)$ for various values of x, assuming $m = 1.33$ (fine-scale oscillations in the curves for large x have been smoothed out by allowing x to vary over a narrow range). The vertical scale is logarithmic but otherwise arbitrary; each curve has been displaced upward from the previous one for clarity. Note increasing asymmetry and complexity of phase functions with increasing x. The topmost curve ($x = 10,000$) is very similar to that predicted by geometric optics except for the narrow forward and backward peaks at 0° and 180°. See Figs. 12.8 and 12.9 for polar plots of some of these same curves.

For slightly larger x, there is a tendency for the phase function in the forward direction $\Theta < 90°$ to have larger amplitude than in the backward direction.

By the time we get to $x = 3$, we have a broad lobe of enhanced scattering for Θ between about 0° and 40°. Within that range, the amplitude of $p(\Theta)$ is around a factor of 100 larger than it is for Θ between 120° and 180°. Now watch this forward-scattering lobe carefully as we move upward on the figure — *it becomes both narrower and more intense with increasing* x. In fact, for very large x, this so-called *forward diffraction peak*, starts to resemble a δ-function and falls right on y-axis in Fig. 12.7, so that it can no longer be distinguished.

At the same time as the forward scattering peak gets narrower with increasing x, the rest of the phase function becomes more complex, exhibiting an ever greater number of ripples. By the time we get to $x = 100$, we start to see unmistakable signs of an enhanced scattering feature near $\Theta = 140°$. This feature also sharpens and intensifies dramatically with increasing x, until there is nearly a hundred-fold difference between the amplitude of the peak at $\Theta = 137°$ and the "floor" of the valley at just a slightly smaller

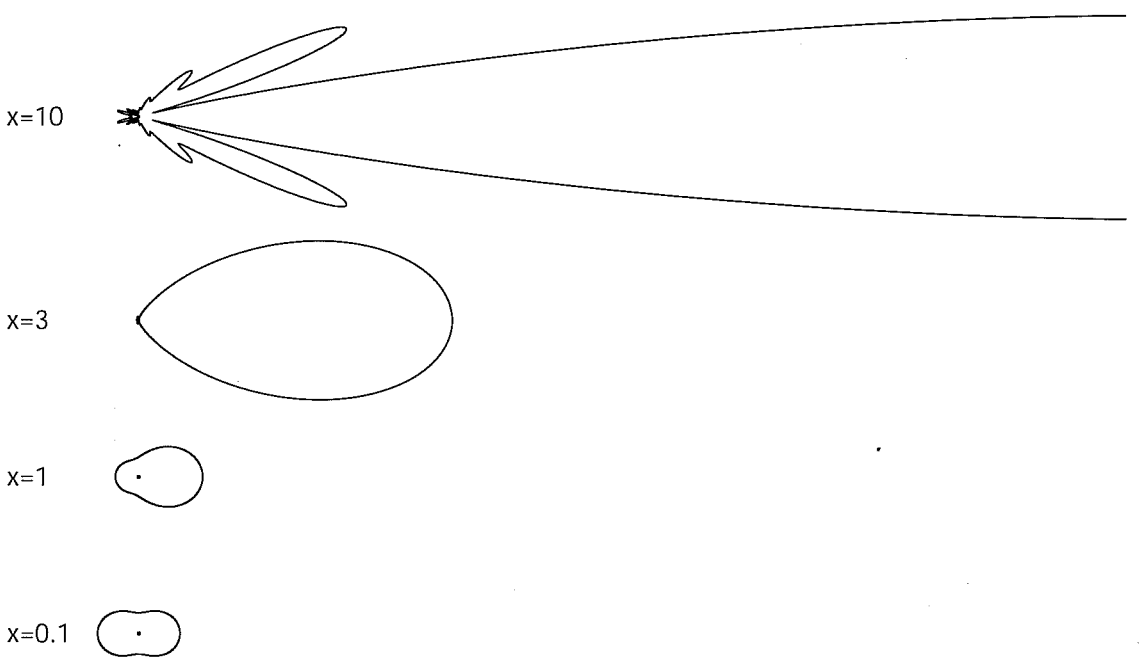

Fig. 12.8: Polar plots of the Mie-derived scattering phase function $p(\Theta)$ for selected values of x.

angle! This feature is the *primary rainbow* whose existence was previously explained in section 4.3.1 using the ray tracing method (Fig. 4.8) and assuming a single internal reflection of the ray. The slightly weaker peak at $\Theta = 130°$, just to the left of the primary rainbow, is the secondary rainbow, which is associated with rays undergoing two internal reflections in the sphere.

In summary, the Mie solution, which is based on an infinite series solution of the EM wave equation with suitable boundary conditions, yields results which basically converge to the geometric optics results, once we let x get large enough. In fact, for $x > 2000$ or so, we have crossed out of the range of x for which Mie theory is traditionally applied (see Fig. 12.1). Even for very large x, however, there are aspects of scattering by particles that geometric optics alone can never explain, such as the forward diffraction peak as well as the intensified scattering near 180° known as the *glory*.

The polar plots in Fig. 12.8 and Fig. 12.9 provide an alternative way of visualizing the evolution of the phase function with increasing x. In the first of these, the amplitude of the phase function is proportional to the distance along a particular radial at angle Θ, with $\Theta = 0$ pointing horizontally to the right. For $x = 0.1$ we again have the symmetric Rayleigh phase function; you'll probably recognize the shape from Figs. 12.2 and Figs. 12.3. For even modest increases in x, the asymmetry quickly becomes very pronounced. By the time we reach $x = 10$, the forward scattering lobe is already so intense that it no longer fits on the page!

For larger x, we can tame the extreme features of the phase function by making the radial amplitude proportional to the *logarithm* of $p(\cos\Theta)$ (Fig. 12.9). Among other things, these plots allow us to clearly see, for the first time, what's happening at $\Theta = 0°$ and $\Theta = 180°$. There are a few features that deserve special mention, because they are associated with commonly observed optical phenomena:

Forward Diffraction Peak

We have already mentioned the strong forward scattering that occurs in connection with larger particles, spherical or not. This phenomenon is readily observable in daily life. It is much harder to

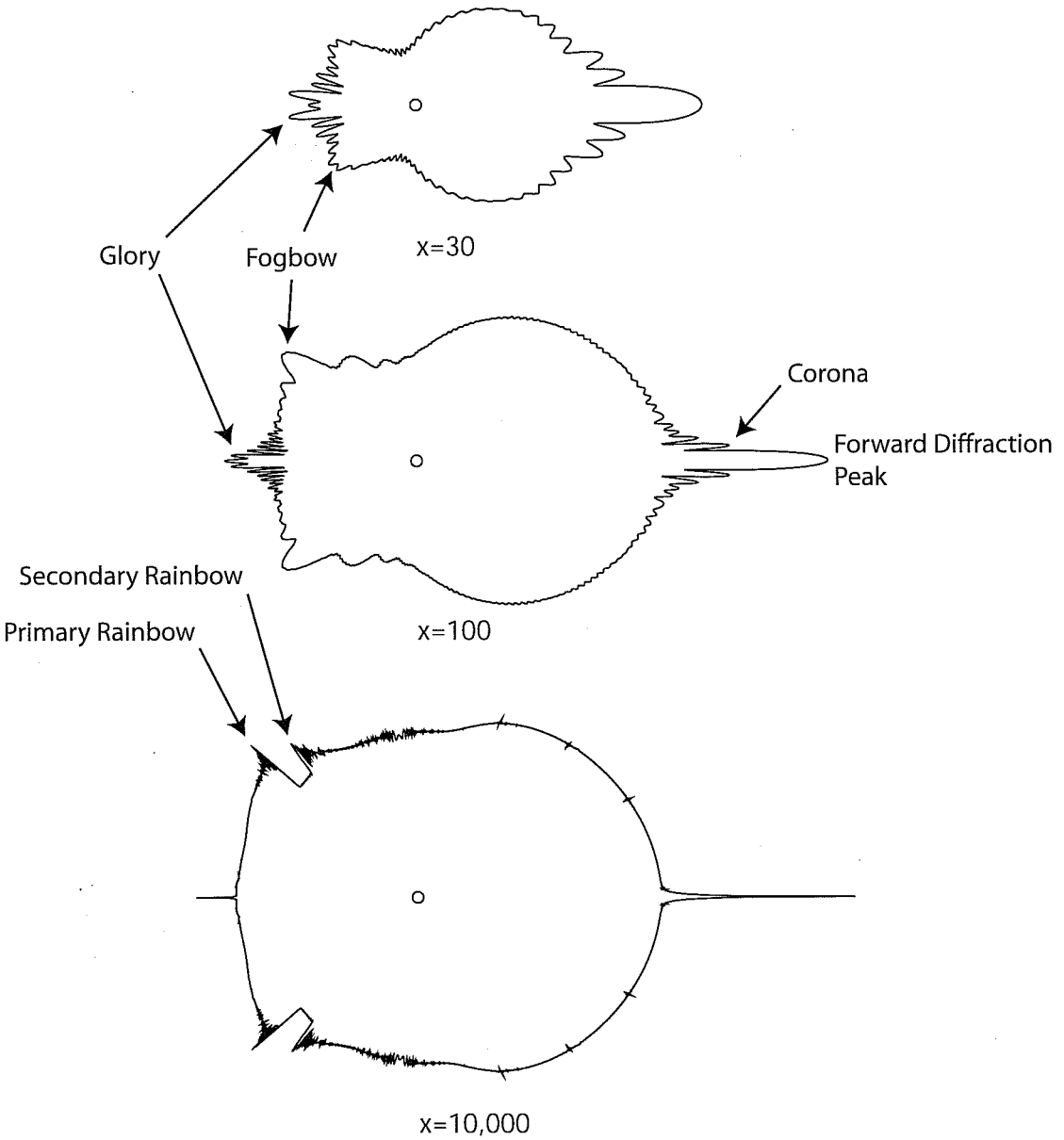

Fig. 12.9: Similar to Fig. 12.8, but plotted as $\log[p(\Theta)]$ so as to better accommodate the extreme variations in the amplitude of the phase function for large x. Commonly observed optical features associated with the phase function are indicated. Note the δ-function-like characteristic of the forward and backward peaks for the largest values of x.

see through the glare of a dirty windshield when driving toward the sun than away. Dust particles settling through a shaft of sunlight in a room are easiest to spot when looking generally toward the source of the light. The rays of light from the setting sun emerging from a break in the clouds (so-called *crepuscular rays*) are most evident when viewed in the general direction of the sun.

Fig. 12.9 makes much clearer the profound narrowing of the diffraction peak with increasing x. For $x = 10,000$, the peak is so narrow that the scattered radiation it represents might as well be considered as never having been scattered at all. In the geometric optics approximation, this feature doesn't even exist! In fact, while Mie theory predicts $Q_e \approx 2$ in the limit of large x, geometric optics always predicts $Q_e = 1$. The forward diffraction peak is largely responsible for the discrepancy.

Corona

For intermediate values of the size parameter x, the forward diffraction peak is accompanied by number of weaker *sidelobes*. If you were to view the sun through a very thin cloud made up of identical spherical droplets with x of order 100 or less, you would see a series of closely spaced rings immediately surrounding the light source. Moreover, because the precise angular position of the rings depends on wavelength, the rings would be brightly colored. This optical feature is known as a *corona*.

Coronas observed in real clouds are more diffuse, and less brightly colored, than the corona you would expect from a cloud composed of identical droplets. In fact, one reason colored coronas are rarely observed at all is because few clouds have a sufficiently narrow distribution of drop sizes.[7]

Far more commonly you will just see a diffuse circular bright patch surrounding the sun with little if any coloration. This feature represents a blending of both the forward diffraction peaks and the sidelobes contributed by a variety of different drop sizes.

[7] Another reason, of course, is that only true enthusiasts of optical phenomena take time each day — and risk their eyesight — in order to stare almost directly at the sun in the hope of spotting a spectacular corona!

Glory

The *glory* is in many respects analogous to the forward diffraction peak and the corona, except that it is exactly on the opposite end of the phase function. It is called a "glory" because if you stand on a hill overlooking a fog bank with the sun at your back, you will see a bright patch or ring surrounding the shadow of your head in a manner reminiscent of medieval paintings of saints.

A much more predictable setting for observing glories is as a passenger in an airplane flying above a cloud layer, from whence a bright ring is often seen immediately surrounding the shadow of the airplane. If the airplane is high enough above the cloud layer, the shadow will be too indistinct to see but the glory will be visible nonetheless.

As was also the case for the corona, glories may involve multiple rings and vivid colors, provided only that the range of drop sizes is sufficiently narrow. More commonly, the glory is seen as a fairly indistinct white ring or circular bright patch.

For very large x, the glory narrows to a δ-function-like spike in the exact backscattering direction $\Theta = 180°$. Like the forward diffraction peak, the glory is a feature not predicted by geometric optics, at least for spheres with the index of refraction of water.[8]

Fogbow/Rainbow

We already mentioned the occcurence of sharp spikes in the scattering phase function corresponding to the primary and secondary rainbows. The positions of these features are noted on the polar plot for $x = 10,000$ in Fig. 12.9. For smaller x, the primary rainbow

[8]You have probably noticed that a lot of street signs, license plates, reflective leg straps for bicycle riders, etc., are intensely reflective when the light source is very close to being in line with the object and the observer. For example, when approaching a stop sign at night from a couple of blocks away, your own headlights cause the sign to light up brightly, whereas illumination by light sources in other directions doesn't have nearly as intense an effect. Close examination reveals the presence of *retroreflective* beads, which are simply small spheres with an index of refraction falling between approximately 1.5 and 2.0. For this range of index of refraction, geometric optics is able to explain the unusually strong backscatter as the result of rays that pass into the sphere and experience total internal reflection on the far side.

feature is still present but not nearly as sharp. Because the peak is much more diffuse, the separation of colors (due to varying n_r) will not be nearly as vivid as you find in a "normal" rainbow, and you will instead observe a more or less whitish ring centered on the point opposite the sun (i.e., centered on your own shadow). In this case, a better name for the feature is *fogbow*, because it arises (for visible light) when the water droplets have a size characteristic of fog and clouds rather than rain.

Problem 12.4: Assuming a wavelength $\lambda = 0.5\ \mu$m, which is near the middle of the visible band, determine the water droplet radii corresponding to each of the three phase functions depicted in Fig. 12.9.

12.4 Distributions of Particles

The atmosphere never contains particles of just one size. In performing radiation transfer calculations for clouds and aerosols, it is invariably necessary to start out by determining the combined optical properties of a distribution of particles of varying sizes and, possibly, shapes and compositions. We will limit our attention to the case of varying size only, though the formal extension to shape and composition is straightforward.

In Section 7.4.4, I already introduced the concept of a size distribution function $n(r)$ for cloud droplets. To refresh your memory,

$$n(r)\,dr = \left\{\begin{array}{l}\text{number of droplets (per unit volume of}\\ \text{air) whose radii fall in the range } [r, r+dr]\end{array}\right\} . \quad (12.25)$$

The same concept is applicable to any particle type.

We already saw that the volume extinction coefficient for the distribution of particles described by $n(r)$ is

$$\beta_e = \int_0^\infty n(r) Q_e(r) \pi r^2\, dr . \quad (12.26)$$

In other words, the total extinction β_e is equal to the extinction cross-section contribution from a single particle of radius r multiplied by

the number of particles (per unit volume) having that radius and then integrated over all possible radii.

A completely analogous relationship gives the scattering coefficient

$$\beta_s = \int_0^\infty n(r) Q_s(r) \pi r^2 \, dr \, . \tag{12.27}$$

From there, we immediately have the single-scatter albedo of the distribution as $\tilde{\omega} = \beta_s / \beta_e$.

The combined scattering phase function is the *scattering cross-section weighted average* of the individual phase functions:

$$p(\cos\Theta) = \frac{1}{\beta_s} \int_0^\infty n(r) Q_s(r) \pi r^2 p(\cos\Theta; r) \, dr \, , \tag{12.28}$$

which also implies a combined asymmetry parameter of

$$g = \frac{1}{\beta_s} \int_0^\infty n(r) Q_s(r) \pi r^2 g(r) \, dr \, . \tag{12.29}$$

12.5 Applications to Meteorology, Climatology, and Remote Sensing

12.5.1 The Scattering Properties of Clouds

The radiative properties of clouds, including their ability to reflect and absorb both solar and thermal radiation, depend on their optical depth τ^*, their single scatter albedo $\tilde{\omega}$ and the scattering phase function $p(\cos\Theta)$. These properties in turn depend on the size parameter x and on the complex index of refraction m for the cloud's constituent particles. Both x and m depend on wavelength λ, and x also depends on the droplet radius r. The index of refraction m depends on composition and material phase as well, but for most clouds, there are only two possibilities: liquid water or ice.

For reasonably large x, we already saw that $Q_e \approx 2$, so that the optical thickness τ^* can often be taken to be almost independent of wavelength. The phase function $p(\Theta)$ is adequately characterized for many purposes by the asymmetry parameter g, which we saw tends to hover in the fairly narrow range 0.8–0.9 for x greater than around 10.

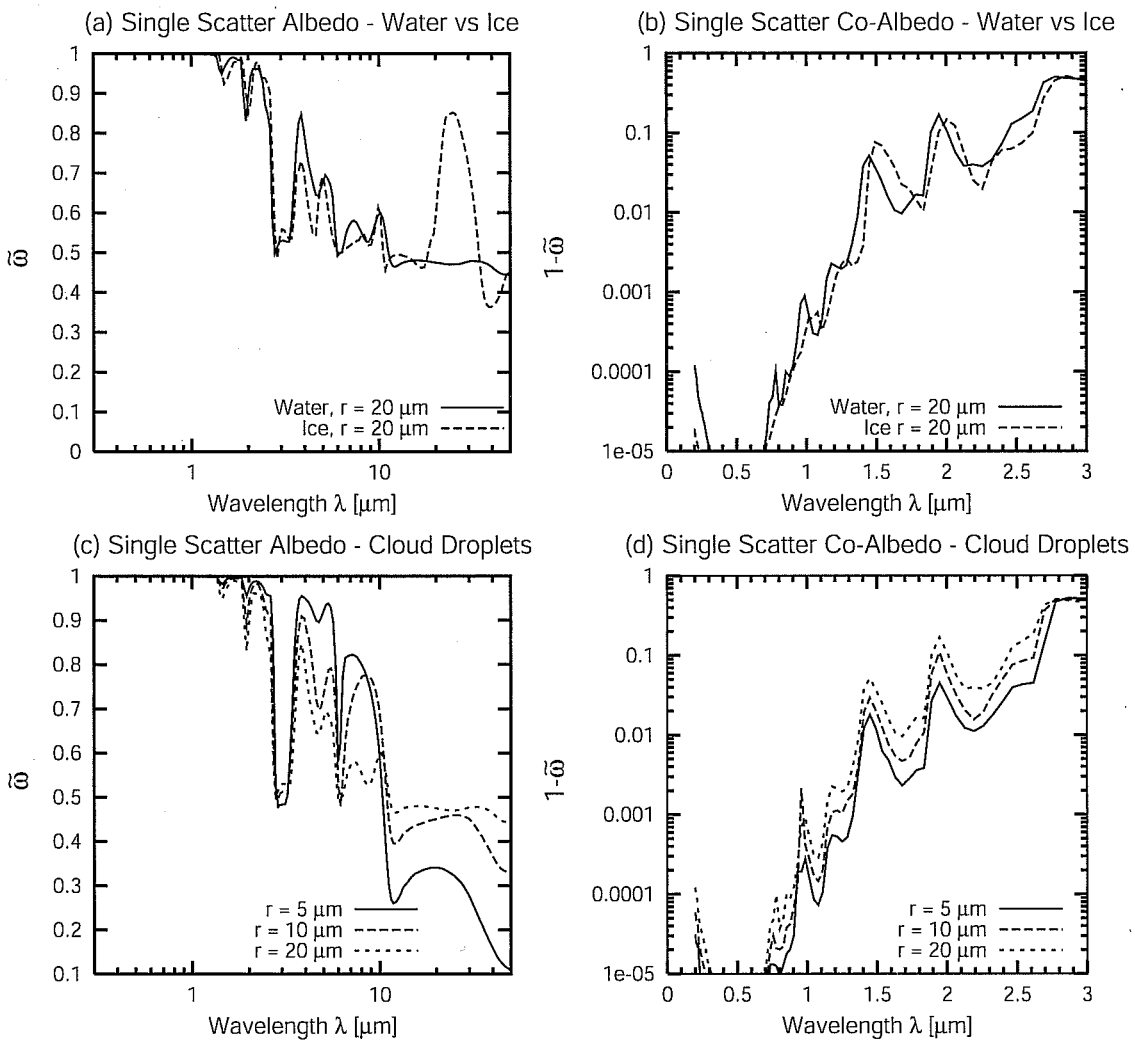

Fig. 12.10: Single scatter albedo (or co-albedo) as a function of wavelength for water and ice spheres of various sizes. The left column depicts $\tilde{\omega}$ over the entire visible, near IR and thermal IR range. The right column depicts the scattering co-albedo (defined as $1 - \tilde{\omega}$) for just the solar band. The top row compares water and ice for particle radius $r = 20$ μm; the bottom row compares water droplets of three different radii (5, 10, and 20 μm).

This leaves the single scatter albedo $\tilde{\omega}$ as the one variable that could potentially have a large influence on how cloud reflectivity/absorptivity varies with λ. And indeed this conjecture is validated by the plots of $\tilde{\omega}$ vs. λ shown in Fig. 12.10. This information is represented in two different ways. The first is by simply plotting $\tilde{\omega}$ on a linear vertical axis, as is done in the two panels in the left column. This is fine for showing the coarse variations of $\tilde{\omega}$ with wavelength but tends to obscure subtle deviations of $\tilde{\omega}$ from exactly one (pure scattering, no absorption), which can nevertheless

be significant for absorption by clouds. Therefore, for the shorter wavelengths where absorption is comparatively weak, we plot the scattering *co-albedo*, defined as $1 - \tilde{\omega}$, on a logarithmic vertical axis.

Here are the basic points you should take away from these plots:

- The visible band ($0.4\ \mu\text{m} < \lambda < 0.7\ \mu\text{m}$) coincides almost exactly with a surprisingly narrow portion of the EM spectrum for which absorption by cloud droplets is, for all practical purposes, zero. You can think of it as an astonishing coincidence that clouds (when viewed from the sunlit side) appear to our eyes as white rather than gray, black, or some other color! As soon as you move into either the UV or near-IR bands, $\tilde{\omega}$ quickly decreases to well below 1, settling into the range 0.5–0.8 for most of the IR band. For even $\tilde{\omega} = 0.8$, the albedo of a thick cloud is only around 15%.

- At several wavelengths, there is a significant difference between the single scatter albedo of a spherical ice particle and that of a water droplet of the same size (top row). For some of these wavelengths, ice particles are less absorptive than the water droplets; for others, the reverse is true. These differences can be exploited by satellite sensors to distinguish ice phase clouds (cirrus) from water clouds[9].

- For most wavelengths, there is a significant dependence of the single scatter albedo on the droplet radius in liquid water clouds (bottom row). As a general rule (although there are exceptions), a larger droplet has lower $\tilde{\omega}$ (i.e., is more absorptive) than a smaller droplet at the same wavelength. Once again, satellite remote sensing techniques can exploit this property to estimate the effective droplet radius r_{eff} in water clouds.

12.5.2 Radar Observations of Precipitation

Radar has become one of the most important observational tools of operational meteorologists as well as hydrologists. Weather radar

[9]The fact that ice particles in clouds are generally *not* spheres complicates the problem somewhat, but the principle is still valid.

allows severe weather systems to be tracked in real-time. It also allows the monitoring of rainfall with far more detail in both time and space than is possible with conventional rain gauges.

The basic principle of operation of a radar system is simple. A transmitter sends out a continuous series of short pulses of microwave radiation. A sensitive receiver then measures the intensity of the backscattered radiation as a function of the time elapsed following each transmitted pulse. The time elapsed Δt is of course just the round trip distance divided by the speed of light c, so that the one-way distance d to the target is given by

$$d = \frac{c\Delta t}{2} \,. \tag{12.30}$$

The backscattered power P_r received by the radar antenna is given by the following proportionality:

$$P_r \propto \frac{\eta}{d^2} \,, \tag{12.31}$$

where η (Greek letter *eta*) is the *backscatter cross-section per unit volume of air*. It is just the sum of the backscatter cross-sections σ_b of all particles in the sampled volume of air V, divided by V:

$$\eta = \frac{1}{V} \sum_i \sigma_{b,i} \,, \tag{12.32}$$

The backscatter cross-section σ_b is closely related to to the more familiar scattering cross-section σ_s, except that it only accounts for radiation scattered exactly backward toward the radar antenna, rather than radiation scattered into all directions. As a matter of fact,

$$\boxed{\sigma_b \equiv \sigma_s \, p(\Theta)|_{\Theta=\pi} \,.} \tag{12.33}$$

Now let's assume that we're dealing with particles that all have the same composition (e.g., liquid water), are spherical in shape, and are distributed in size according to a size distribution function $n(D)$, where D is the droplet diameter. The assumption of spherical shape, while approximate, is reasonable for raindrops that are "not too large."

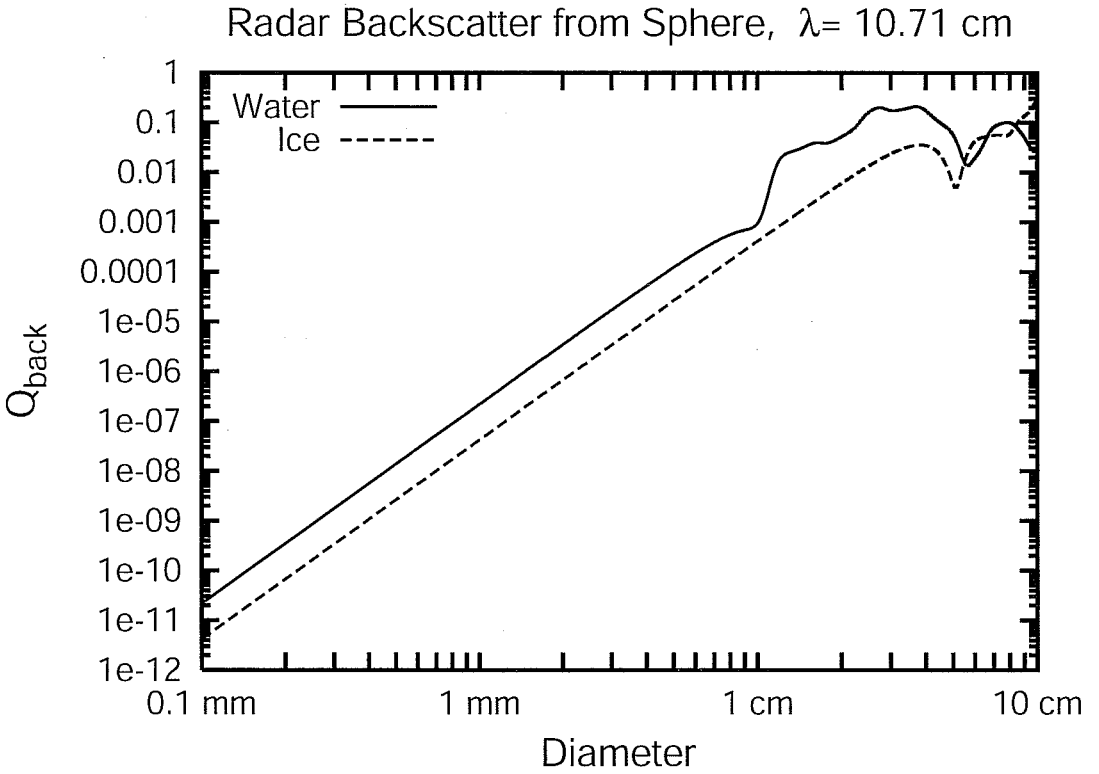

Fig. 12.11: Radar backscatter efficiency Q_b for water and ice spheres at the wavelength of the WSR-88D operational weather radar.

We can then replace the summation in (12.32) with an integral involving $n(D)$ and $\sigma_b(D)$:

$$\eta = \int_0^\infty \sigma_b(D) n(D)\, dD\,, \tag{12.34}$$

or

$$\eta = \int_0^\infty Q_b(D) \left[\frac{\pi}{4} D^2\right] n(D)\, dD\,, \tag{12.35}$$

where the term in square brackets is just the cross-sectional area of a sphere with diameter D, and Q_b is the *backscatter efficiency*.

If our spherical particles happen to have size parameters $x \ll 1$, then we're in the Rayleigh regime. This means that (a) the Rayleigh formula (12.13) for σ_s applies, and (b) the phase function is given by (12.10). Substituting these into (12.33) gives

$$Q_b = 4x^4 \left|\frac{m^2 - 1}{m^2 + 2}\right|^2 . \tag{12.36}$$

If our particles are too large, then Rayleigh theory no longer applies, and we have to calculate σ_b using Mie theory. Fig. 12.11 shows

accurate calculations of Q_b for a wide range of sizes of water and ice spheres. The wavelength $\lambda = 10.71$ cm chosen for these calculations corresponds to that used by the current-generation operational weather radar network in the United States.

You can see that for liquid water spheres up to a diameter of about 6 mm (solid curve), the Rayleigh relationship (12.36) holds to a high degree of accuracy: each decade (factor ten) increase in D corresponds to a four decade (factor 10^4) increase in Q_b. In fact, 6 mm corresponds to a rough upper limit on the observed sizes of raindrops in heavy rain; beyond this size, raindrops tend to be broken up by aerodynamic forces as they fall.

Hailstones can of course become considerably larger than raindrops. It is therefore convenient that the Rayleigh approximation apparently holds up to a diameter of around 3 cm for a pure ice sphere (dashed curve). Note that for any given D in the Rayleigh regime part of the curve, Q_b for pure ice is only 20% of that for liquid water. This difference is due to the substantially smaller value of m for ice in the microwave band, as compared to liquid water[10].

Problem 12.5: Based on the above information, compute the diameter of a spherical hailstone that has the same radar backscatter cross-section σ_b (not Q_b!) as a spherical raindrop with a diameter of 2 mm.

Let's assume that the hydrometeors (e.g. raindrops, hailstones, etc.) that are observed by a 10-cm weather radar all fall in the Rayleigh regime. We can then substitute (12.36) into (12.35) to get

$$\eta = \frac{\pi^5}{\lambda^4} \left| \frac{m^2 - 1}{m^2 + 2} \right|^2 \int_0^\infty n(D) D^6 \, dD \, . \tag{12.37}$$

Substituting this expression back into (12.31), we find that the backscattered power measured by the radar receiver is

$$P_r \propto \left| \frac{m^2 - 1}{m^2 + 2} \right|^2 \frac{Z}{d^2} \, , \tag{12.38}$$

[10]It is worth keeping in mind, however, that growing hailstones often have a coating of liquid water. Even a thin coating of water can drastically alter the radar backscattering properties of an ice particle.

where Z is the *reflectivity factor*, defined as

$$\boxed{Z = \int_0^\infty n(D) D^6 \, dD \, .} \tag{12.39}$$

In other words, the reflectivity factor is numerically equal to *the sum of the sixth powers of the diameters of all of the drops in a unit volume of air.* The standard units of Z used by meteorologists are $[\mathrm{mm}^6\mathrm{m}^{-3}]$. *An estimate of the reflectivity factor Z at each range d along the beam is what most weather radars record and display.*

Because observed values of Z span an enormous range, meteorologists prefer to work with a logarithmic representation of Z, defining a nondimensional unit dBZ, which means "decibels with respect to one standard unit of Z." You convert the reflectivity factor from standard units to units of dBZ as follows:

$$Z\ [\mathrm{dBZ}] = 10 \log_{10}(Z) \, , \tag{12.40}$$

where Z on the right hand side is the numerical value of Z expressed in standard (dimensional) units of reflectivity. Thus, an increase in reflectivity by 10 dBZ corresponds to a factor ten increase in Z expressed in standard units. An increase of 30 dBZ implies a thousand-fold increase in reflectivity.

Problem 12.6: Depending on range, a typical weather radar can measure reflectivities from as low as -20 dBZ to as high as 70 dBZ. In terms of physical units, what is the ratio of the two reflectivity factors?

In converting the received power P_r to an estimate of the reflectivity factor Z, the radar processing software assumes a value of m appropriate to liquid water in (12.38). The displayed quantity is therefore actually better regarded as an *equivalent reflectivity factor* Z_e which may or may not be equal to the *true* reflectivity factor Z defined by (12.39), depending on whether the targets are liquid water or something else, like ice. If the particles are in fact ice, then

$$Z_e \approx 0.20 Z \, . \tag{12.41}$$

Problem 12.7: During a particular (and peculiar) rainstorm, each cubic meter of air contains 1000 falling drops, each of identical diameter D. (a) Compute the reflectivity factor Z, assuming $D = 1$ mm. (b) Repeat for $D = 2$ mm. (c) By what factor did Z increase on account of a mere two-fold increase in D? (d) Express your answers to (a)–(c) in units of dBZ. (e) If you replace the liquid raindrops with ice spheres of the same size, by how many dBZ will the radar-estimated effective reflectivity Z_e be reduced? (f) Notwithstanding Eq. (12.41), hailstorms are often recognized on radar displays by virtue of their anomalously *high* Z_e. Why?

In actual rainfall, drops do not all have one size but rather are distributed over a wide range of sizes. Because of the D^6 dependence in Z, observed reflectivities are heavily influenced by the few largest drops in the volume of air. A single drop with a diameter 5 mm reflects more microwave radiation than 15,000 drops of 1 mm diameter! And clouds, with their typical droplet diameters of around 20 μm, are completely invisible to all but the most sensitive radars, despite typical droplet concentrations in excess of 10^8 m^{-3}.

Problem 12.8: From the information given above concerning cloud droplets, find a typical reflectivity factor Z for clouds, expressed in dBZ.

Radar Rainfall Estimation

Raindrops passing through the air eventually reach the surface, and the rate at which water is deposited (depth per unit time) is known as the *rainfall rate* R. One of the most important applications of radar is the operational estimation of accumulated rainfall for agricultural and hydrological purposes.

Unfortunately, there is no unique relationship between the rainfall rate and the relative number of larger and smaller droplets present in the column of air. Consequently, there can be no unique relationship between radar reflectivity Z and rain rate R. However, we know from experience that heavier rainfall *tends* to be associated

with a greater number of large raindrops, whereas light rain is *usually* characterized by smaller drops. *On average*, therefore, we expect heavy rain rates to be associated with large Z and light rain rates to give rise to correspondingly weaker radar echoes.

Field observations of raindrops have revealed that the dropsize distribution $n(D)$ for rain is often reasonably well approximated by

$$n(D) = N_0 \exp(-\Lambda D) , \tag{12.42}$$

where N_0 and Λ are parameters that are functions of the rain rate R. In fact, the most widely used model of the above form is known as the *Marshall-Palmer size distribution*, after the researchers who developed it. In the Marshall-Palmer distribution, N_0 is a constant and $\Lambda = aR^b$, where the parameters a and b were chosen so as to maximize the agreement between the above size distribution function and a large number of actual observations of drop sizes at various rain rates.

It is beyond the scope of this text to discuss the M.-P. distribution in detail, except to note that, when it is substituted into (12.39) and combined with suitable assumptions about raindrop fall speed as a function of D, it is possible to obtain the following Z–R relationship:

$$Z = 200R^{1.6} , \tag{12.43}$$

where R is assumed to be given in mm hr^{-1}, and Z is in standard units of mm^6 m^{-3}. Other assumed (or measured) drop size distributions usually lead to Z–R relationships having a similar form, but with different values for the two numerical coefficients.

Problem 12.9: Use the Marshall-Palmer Z–R relationship above to estimate the rain rates R associated with displayed radar reflectivities of (a) 10 dBZ, (b) 30 dBZ, and (c) 50 dBZ.

12.5.3 Microwave Remote Sensing and Clouds

Microwave radiometers operating at various frequencies from 3 to 183 GHz are assuming an increasingly prominent role in the satellite remote sensing of the atmosphere. One of the main attractions of

the microwave band is the relative transparency of clouds at these wavelengths, so that some properties of the surface and of the atmospheric column can be estimated under nearly all-weather conditions.

At even the high end of the frequency range given above, the wavelength λ is a relatively long 3 mm which, for typical 10 μm radius cloud droplets, gives size parameter $x \approx 0.02$. This is so small that we can ignore scattering, and the mass extinction (absorption) coefficient k_L of cloud liquid water is accurately given by (12.19). Figure 12.12 shows how k_a varies with frequency over the microwave band.

Consider a microwave radiometer at ground level viewing vertically incident radiation emitted by the atmosphere. In the microwave band, the Rayleigh-Jeans approximation allows us to work with brightness temperature T_B as a convenient stand-in for radiant intensity, with $T_B = \varepsilon T$, where ε is the emissivity of a surface or atmospheric layer, and T is its physical temperature (see section 6.1.4).

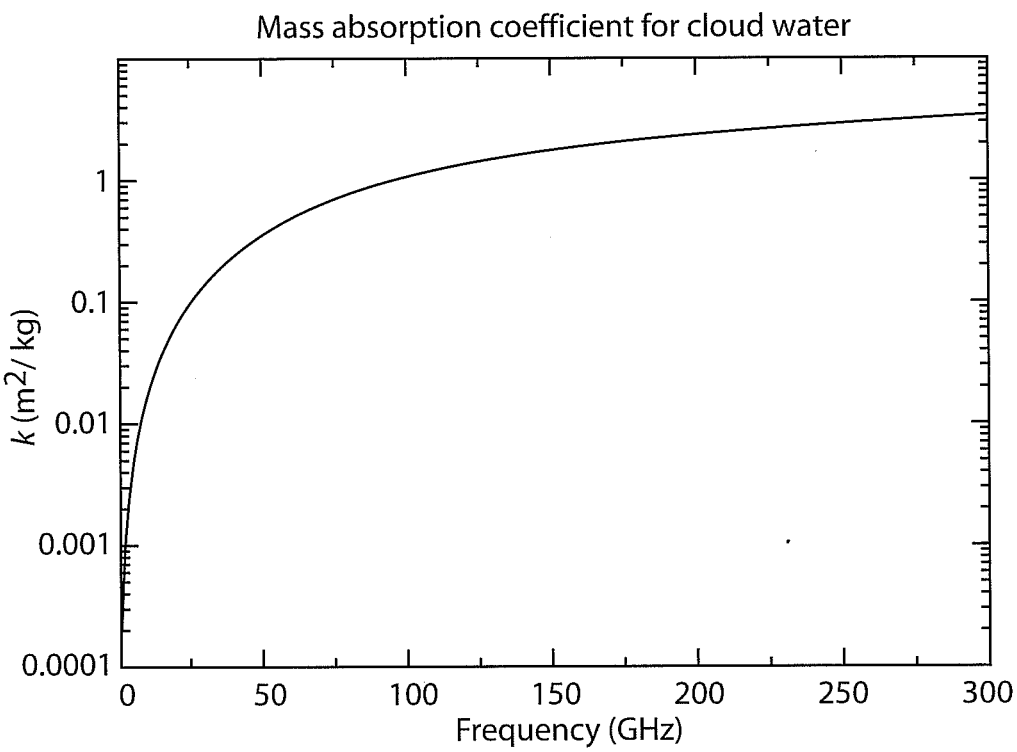

Fig. 12.12: The mass absorption coefficient for cloud water at microwave frequencies.

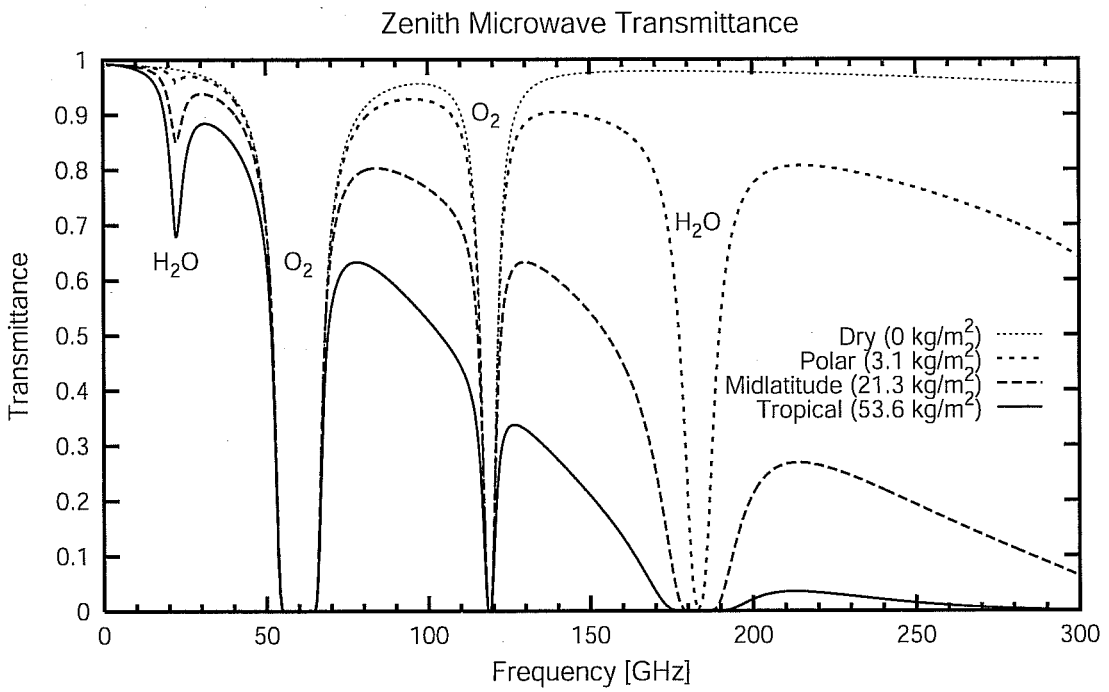

Fig. 12.13: Zenith microwave transmittance of the cloud-free atmosphere for different models of atmospheric temperature and humidity. The vertically integrated water vapor content associated with each model is given in parentheses.

If we assume for the moment that the cloud-free atmosphere is perfectly transparent (it is not) and that there is a single cloud layer with average temperature T and total vertically integrated cloud liquid water L, then the measured brightness temperature is given approximately by

$$T_B = \varepsilon T = [1 - t(L)]\, T = [1 - \exp(-k_L L)]\, T\,. \qquad (12.44)$$

You could then use your upward-looking microwave radiometer to estimate the cloud water path by simply (i) solving the above equation for L, (ii) assuming something reasonable for T, and (iii) plugging in the observed brightness temperature T_B.

The reality is of course slightly more complicated. In particular, there are two other atmospheric constituents that always contribute additional absorption and emission in the microwave band: water vapor, and oxygen (Fig. 12.13). If we stay well away from the 60 GHz and 118 GHz absorption bands due to oxygen, then the reduction in transmittance due to the dry atmosphere alone is only a few percent. Furthermore, since the surface air pressure at any given location, and therefore the total column oxygen content,

varies only by about 5%, we can get away with assuming a fixed optical depth τ_O due to oxygen.

Water vapor is a bigger problem, because atmospheric column vapor content V varies from very low ($\sim$1 kg m^{-2}) in dry polar air masses to rather high (up to 60 kg m^{-2}) in humid tropical air masses. In order to limit the total optical depth due to water vapor, let's confine our attention to the spectrum below about 40 GHz, so that even in the worst case, we still have a zenith transmittance of at least 60% or so. That way, the atmosphere will never become so opaque due to water vapor that it becomes hard to see changes in opacity due to cloud water.

If we assume that the mean emitting temperature of the atmospheric water vapor and oxygen isn't *too* different from that of the cloud layer, then we can write

$$T_B \approx [1 - \exp(-\tau)]\, T\,, \tag{12.45}$$

where the total atmospheric optical depth is approximated as

$$\tau \approx \tau_O + k_L L + k_V V\,, \tag{12.46}$$

and k_V is the column-averaged mass absorption coefficient of water vapor. We can divide through by T, rearrange, and take the logarithm of both sides to get

$$y \equiv \log\left(\frac{T - T_B}{T}\right) \approx -k_L L - k_V V - \tau_O\,. \tag{12.47}$$

Given a reasonable value for T, the new variable y is a known function of the observed T_B. The definition of y is convenient because it turns out to be a simple linear function of our two unknowns V and L. Unfortunately, we have one equation in two unknowns, and so a measurement of T_B at a single wavelength is not sufficient to uniquely determine both variables.

Let's therefore design our radiometer to measure T_B at two different frequencies ν_1 and ν_2. We can then write our equation in matrix form as

$$\begin{bmatrix} y_1 \\ y_2 \end{bmatrix} = -\begin{bmatrix} k_{L,1} & k_{V,1} \\ k_{L,2} & k_{V,2} \end{bmatrix} \begin{bmatrix} L \\ V \end{bmatrix} - \begin{bmatrix} \tau_{O,1} \\ \tau_{O,2} \end{bmatrix}\,. \tag{12.48}$$

We now have two linear equations in two unknowns. In principle, we can solve for L and V as follows:

$$\begin{bmatrix} L \\ V \end{bmatrix} = - \begin{bmatrix} k_{L,1} & k_{V,1} \\ k_{L,2} & k_{V,2} \end{bmatrix}^{-1} \begin{bmatrix} y_1 + \tau_{O,1} \\ y_2 + \tau_{O,2} \end{bmatrix}, \tag{12.49}$$

assuming that the inverse of the matrix of absorption coefficients $\mathbf{K}$ exists.

Mathematically speaking, the inverse exists if the determinant $\|\mathbf{K}\| \neq 0$, a condition that is almost guaranteed to be satisfied for any pair of distinct microwave frequencies. *Practically* speaking, however, the mere existence of an inverse is not enough! Why not?

Recall that (12.47) was presented as an *approximate* model of the dependence of y on L and V. This suggests that we should modify (12.49) to allow for the likelihood of errors ϵ_i in the relationship:

$$\begin{bmatrix} L' \\ V' \end{bmatrix} = - \begin{bmatrix} k_{L,1} & k_{V,1} \\ k_{L,2} & k_{V,2} \end{bmatrix}^{-1} \left\{ \begin{bmatrix} y_1 + \tau_{O,1} \\ y_2 + \tau_{O,2} \end{bmatrix} - \begin{bmatrix} \epsilon_1 \\ \epsilon_2 \end{bmatrix} \right\}, \tag{12.50}$$

where L' and V' are now *estimates* of the true L and V. The *estimation error* can then be written

$$\begin{bmatrix} L' - L \\ V' - V \end{bmatrix} = \begin{bmatrix} k_{L,1} & k_{V,1} \\ k_{L,2} & k_{V,2} \end{bmatrix}^{-1} \begin{bmatrix} \epsilon_1 \\ \epsilon_2 \end{bmatrix}. \tag{12.51}$$

The goal of a remote sensing technique, of course, is to make sure that the estimation errors are as small as possible. In this instance, it means ensuring that the matrix $\mathbf{K}^{-1}$ does not excessively "amplify" the model and/or instrument errors ϵ_i. Since the magnitude of $\mathbf{K}^{-1}$ is proportional to $1/\|\mathbf{K}\|$, it follows that we require not only that $\|\mathbf{K}\|$ be nonzero (the strict mathematical requirement for invertibility) but that it be as large as possible!

In plain English, we want our two sensor channels to respond in substantially different ways to L and V, so that the opacity contributions of each constituent can be separated with as little ambiguity as possible. Now, regardless of frequency, $k > 0$ for both L and V, so the most we can hope for is that one channel should have a proportionally larger response to V than to L, while for other channel the reverse should be true. Examination of Figs. 12.12 and 12.13 suggests the way to achieve this: Choose one channel to fall on or

near the center of the water vapor absorption line at 22.235 GHz; choose the second channel to fall between 30 and 40 GHz, where water vapor absorption is much weaker than for the first channel but liquid water absorption is significantly stronger. This is in fact what is done in the design of commercial two-channel microwave radiometers, though the precise choice of frequencies depends on a more sophisticated analysis than we have offered here.

Several other subtleties have also been glossed over here with respect to the *optimal inversion* of radiometric measurements; these are best left to a course in remote sensing. Suffice it to say that an explicit matrix-inverse method, as described above, is usually less satisfactory than a statistical or semi-statistical method that is chosen so as to minimize the average squared error over the widest possible range of atmospheric conditions.

Problem 12.10: Assume that you have an upward-looking microwave radiometer with channels at 23.8 GHz and 31.4 GHz. For the first frequency, take $k_{L,1} = 0.087$, $k_{V,1} = 0.0052$, and $\tau_{O,1} = 0.02$. For the second frequency, take $k_{L,2} = 0.15$, $k_{V,2} = 0.0021$, and $\tau_{O,2} = 0.03$. All values for k are in units of m^2/kg. Assume a mean atmospheric temperature $T = 280$ K.

(a) Approximately what brightness temperature T_B should each channel observe in a perfectly dry atmosphere, with $V = L = 0$?

(b) Repeat your calculation for $V = 60$ kg m^{-2}, which is typical of a humid tropical atmosphere. Leave $L = 0$ (i.e., no cloud).

(c) Repeat your calculation again, this time assuming $L = 0.3$ kg m^{-2}, which is typical of a fairly thick nonprecipitating stratocumulus layer.

(d) Derive a retrieval algorithm for the estimation of V. The final algorithm should have the form $V' = a_1 \log(T - T_{B,1}) + a_2 \log(T - T_{B,2}) + a_3$. Provide the coefficients a_i to four significant figures.

(e) Test your algorithm by applying it to your results from parts (a), (b), and (c). Do you recover the correct values of V in each case?